



Article

Tribological Behavior of Reinforced PTFE Composites and Un-Reinforced Polyketone-Based Materials against Coated Steel

Federica Amenta ^{1,2,*} , Giovanni Bolelli ^{1,3,4}, Stefano De Lorenzis ¹, Alessandro Bertarini ² and Luca Lusvarghi ^{1,3,4} 

¹ Department of Engineering “Enzo Ferrari”, Università di Modena e Reggio Emilia, Via Pietro Vivarelli 10/1, 41125 Modena, Italy; giovanni.bolelli@unimore.it (G.B.); delorenzis.stefano@gmail.com (S.D.L.); luca.lusvarghi@unimore.it (L.L.)

² ATP S.p.A., Via Austria 12/14/16, 41100 Modena, Italy; a.bertarini@atpgroup.it

³ InterMech—MO.RE. Centro Interdipartimentale per la Ricerca Applicata e i Servizi nel Settore della Meccanica Avanzata e della Motoristica, Università di Modena e Reggio Emilia, Via Pietro Vivarelli 2, 41125 Modena, Italy

⁴ Consorzio Interuniversitario Nazionale per la Scienza e Tecnologia dei Materiali (INSTM), Local Unit: Università di Modena e Reggio Emilia, Via Pietro Vivarelli 10/1, 41125 Modena, Italy

* Correspondence: f.amenta@atpgroup.it; Tel.: +39-059-213-0711; Fax: +39-059-314-085

Abstract: In this study, two polymeric materials were tested in a dry rotating “pin-on-disc” configuration against differently coated surfaces, to evaluate their tribological response under conditions, such as those of rotary lip seals, and to identify the wear mechanism of each coupling. A PTFE based material, reinforced with glass fibers and a solid lubricant, and unreinforced polyketone were tested against a chromium oxide coating deposited by plasma thermal spraying, a CrN/NbN superlattice coating deposited by Physical Vapor Deposition (PVD), and a Diamond-Like Carbon (DLC) coating obtained through a hybrid PVD/PECVD (Plasma-Enhanced Chemical Vapor Deposition) process. The PTFE matrix composite offers better overall performance, in terms of specific wear rates and friction coefficients than polyketone. Although the tribological behavior of this material is generally worse than that of the PTFE matrix composite, it can be used without reinforcing fillers. Our analysis demonstrates the importance of transfer-film formation on the counter-surfaces, which can prevent further wear of the polymer if it adheres well to the counterpart. However, the tribofilm has opposing effects on the friction coefficient for the two materials: its formation leads to lower friction for PTFE and higher friction for polyketone.

Keywords: sliding wear; PTFE; polyketone; friction coefficient; coated surfaces; seals



Citation: Amenta, F.; Bolelli, G.; De Lorenzis, S.; Bertarini, A.; Lusvarghi, L. Tribological Behavior of Reinforced PTFE Composites and Un-Reinforced Polyketone-Based Materials against Coated Steel. *Lubricants* **2022**, *10*, 5. <https://doi.org/10.3390/lubricants10010005>

Academic Editor: Jinyang Xu

Received: 7 December 2021

Accepted: 28 December 2021

Published: 31 December 2021

Publisher’s Note: MDPI stays neutral with regard to jurisdictional claims in published maps and institutional affiliations.



Copyright: © 2021 by the authors. Licensee MDPI, Basel, Switzerland. This article is an open access article distributed under the terms and conditions of the Creative Commons Attribution (CC BY) license (<https://creativecommons.org/licenses/by/4.0/>).

1. Introduction

Polymeric materials typically have low dimensionless wear coefficients [1] and low to moderate friction [2,3] under suitable operating conditions in their sliding contact with metals [4]. This is mainly due to their chemical inertness and low surface energy (see typical surface energy values in [5]), and because many create a transfer film on the antagonist surface, which mediates the contact [6].

The sliding resistance in polymeric materials is hindered by the need to limit the contact temperature [6]. An increase in temperature can lead to a rapid decrease in mechanical properties due to the low melting (or softening) point, and these materials are sensitive to surface heating by friction, which is further facilitated by their low thermal conductivity (typically between 0.1 and 0.3 W/mK [4]). Localized heating can cause an excessive softening of the material, and in some cases, the chemical degradation of the polymer.

Polytetrafluoroethylene or PTFE is a high-performance semicrystalline thermoplastic polymer [2] that is known for its ability to produce a low friction coefficient when combined

with many other engineering materials. Thus, it is used in many sliding wear applications, ranging from roller bearing cages to sliding bearings, seals, etc. [2].

Like other linear chain polymers (e.g., polyamides and acetal resins), PTFE has self-lubricating properties. Due to the regular and linear structure of the polymer chains, the transfer layer formed by these materials contains polymer molecules stretched along the sliding direction [6–8]. Thus, in the contact area a polymer–polymer interaction rather than a polymer–ceramic/metal interaction occurs, and due to the absence of polar groups, the adhesion is very low, which leads to the low values of the friction coefficient (typically between 0.03 and 0.15). During the formation process of the transfer film, the polymer layer reaches a thickness limit and “blocks” of PTFE become detached and are elongated in the sliding direction. The periodic detachment of a part of the transfer film and its restoration during sliding can cause an increase in the PTFE wear rate, even in low friction conditions [6–8].

Despite its interesting tribological properties, unreinforced PTFE is rarely used in its pure form for highly loaded sliding contacts. Various composites reinforced with inorganic or organic (polymeric) additives have been developed and are commercially available [9]. Reinforcements first reduce the wear rate of pure PTFE by increasing the surface hardness, because after running in, most of the contact is borne by the hard reinforcements. The size of the debris “sheets” removed from PTFE is also reduced when reinforcements are present [4]. Second, the adhesion of the transfer layer to the countersurface is improved when debris from the reinforcement is mixed with PTFE-based debris. Ensuring delamination of the transfer-film does not frequently occur is important, as this counteracts the high level of wear of pure PTFE [5].

Glass fibers are commonly used inorganic reinforcements, due to their low cost and low density. They can be applied in various percentages and combined with other fillers [6]. T.A. Blanchet found that glass fibers reduce wear by interrupting subsurface deformation and crack propagation, which would otherwise lead to large wear sheets under severe sliding conditions [8]. M. Conte suggested that the use of glass fibers in a PTFE matrix can improve the tribological properties by reducing abrasiveness [8]. Recent studies have further explored how additions of secondary reinforcement phases, such as solid lubricants (graphite flakes or MoS₂), nanoparticles, and whiskers, affect the tribological response of the composites [7,10–17].

Polyketone (PK) is a semi-crystalline polymer with a melting temperature of between 220 and 260 °C. It has a lower density than PTFE (between 1.25 and 1.38 g/cm³), excellent resistance to many chemical agents, and high impermeability to oxygen and other gases. PK has excellent mechanical properties even when not filled, unlike unreinforced PTFE. Its Young’s modulus is around 1.4 GPa [17], which makes it suitable for structural and tribological applications without reinforcement. Using polyketones in tribological systems has only recently been considered, as research into them is limited compared to that of PTFE, whose tribological properties have been investigated in many scientific studies.

Some [17,18] show that the wear rate of PK increases with pressure, in contrast with the response of PTFE, along with the sliding speed (a linear increase). The coefficient of friction of polyketones increases when the sliding speed increases and decreases when the applied pressure increases. Thus, polyketones can be potentially used in tribosystems with low sliding speeds and low pressure, where they demonstrate the best wear resistance. Further, PKs are less expensive than PTFE composites, as they can be created more simply and used without reinforcing phases, as these can lead to an unwanted abrasive action. Polyketones can therefore be considered a potential alternative to PTFE-based composites, for example as lip seals in food processing/packaging equipment, where chemically inert and non-toxic materials are required in food-contact parts. However, under low applied pressure conditions, the coefficient of friction is at its maximum, unlike PTFE, which has a very low coefficient of friction and a comparable wear rate. Their performance levels should therefore be compared to confirm that PK has tribological applications.

The counter surface is also important to the tribological response of polymer materials, and, in particular, the influence of the counterface roughness. This has been extensively

examined in research papers and described in textbooks [4,6,19–21], and its effect is dependent on the sliding conditions and the type of polymer-based material. For example, it has been reported [4] that steel surfaces with Ra of 0.2–0.4 μm provide optimal conditions for the formation of a transfer layer of polymer, in which the values of both friction and wear are at their lowest. With higher roughness values, the asperities of the antagonist generally have an abrasive action that increases the wear rate and the coefficient of friction. The release of coarse debris patches also results in the formation of an irregular and thus less effective transfer film [4,19,22–24]. The specific trends are, however, very much dependent on the type of polymer and on the possible presence of reinforcements (e.g., particles, fibers) and/or functional additives (e.g., solid lubricants). For Ra values lower than 0.2–0.4 μm , the transfer of polymeric material to the counterpart is not always triggered and the tribofilm is not properly developed [4,19], although some studies report stable and low friction and wear, even at Ra < 0.1 μm [22,23].

The cited works mainly examined steel counterfaces, and thus the effects of coated counterfaces are relatively unknown. Surberg et al. [25] characterized the sliding wear response of fiber-reinforced PTFE composites against various counterfaces, including a diamond-like carbon (DLC) film, a thermal spray WC-based hard metal coating, electroplated hard chromium, and grit-blasted steel. Their results [25] indicated that some coatings behave differently when against polymers than against metal or ceramic materials. For example, DLC, which is known for producing very low friction in sliding contacts with metallic or ceramic counterparts [26], does not appear to minimize friction against a PTFE-based composite [25] in comparison with other counter surfaces examined. Thus, confirming the sliding wear behavior of polymer-based materials against diverse counter-surfaces is important, because findings specific to a tribosystem cannot be generalized easily while they represent current industrial practices.

Thus, our research is aimed at extending the limited knowledge of how the tribological response of polymers and polymer-based composites is affected by their complex interactions with different types of counter surfaces. The sliding wear behavior of PTFE composites reinforced with either glass or carbon fibers against both uncoated stainless steel and a plasma-sprayed Cr_2O_3 coating has been previously investigated [27].

We extend this research by considering further material combinations. Unreinforced Polyketone and the PTFE-based composite reinforced with glass fibers were found to be conducive to lower friction than carbon fibers, if not lower wear [27], and were further functionalized with hexagonal boron nitride (h-BN). These materials were then combined with three distinct counterparts that are commonly used as lip seal counter-surfaces in food processing systems: one thick ($\approx 200 \mu\text{m}$) plasma-sprayed Cr_2O_3 coating, which was similar to that used in [27]; and a CrN/NbN multi-layer and a Diamond-Like Carbon (DLC) film, which are thin (<5 μm) films deposited through physical and/or chemical vapor processes. These materials are known for their sliding wear resistance [28–33] and are suitable for food-contact applications [34–36].

We, therefore, aim to identify optimal tribological couplings (polymer material—counter-surface) to obtain low friction and/or low wear in low-speed contacts with a PTFE-based composite and an unreinforced PK.

2. Experimental

2.1. Materials

A PTFE-based composite produced by ATP S.p.A., and an unreinforced polyketone (PK) provided by an external supplier were tested (Table 1). These materials are commonly used in the production of sliding lip seals for food-contact applications.

Table 1. Polymeric materials tested in this work.

Name	Supplier	Matrix	Filler (wt.%)
SYNTEK 439	ATP S.p.A.	PTFE	15% glass fibers + 2% hexagonal boron nitride
SYNTEK PKE	Röchling Engineering Plastics	Polyketone	no filler

Short glass fibers were added to the PTFE matrix to improve its mechanical strength and wear resistance. Hexagonal boron nitride (h-BN) is a known solid lubricant that possesses a lamellar structure, such as graphite and molybdenum disulfide. Although it is less effective as a lubricant [37], it is chemically stable and non-toxic [38] and is thus suitable for food-contact applications. Its white color [37] is also beneficial commercially, as visual workplace cleanliness is extremely important in applications in the food industry.

The composite was obtained by mixing specific amounts of PTFE powder and fillers. Mixed powders were compression molded at room temperature into a “green” body and subsequently sintered at 360–375 °C.

The nominal physical and mechanical properties of Syntek 439 and Syntek PKE are given in Table 2.

Table 2. Nominal properties of the polymeric materials used in this study.

	Syntek 439	Syntek PKE
Density [g/cm ³]	2.18–2.26	1.25
Hardness—Shore D	≥55	≥75
Tensile strength [MPa]	≥20	70
Elongation at break (%)	≥230	70

All polymeric materials were turned into cylindrical pins with a 2 mm-radius spherical tip (Figure 1) for pin-on-disc sliding wear tests.

**Figure 1.** Example of the specimen used for the pin-on-disc test.

Their counterparts were steel discs with various commercially available coatings (Figure 2). The type of coatings, their hardness, and post-finishing treatments are shown in Table 3.

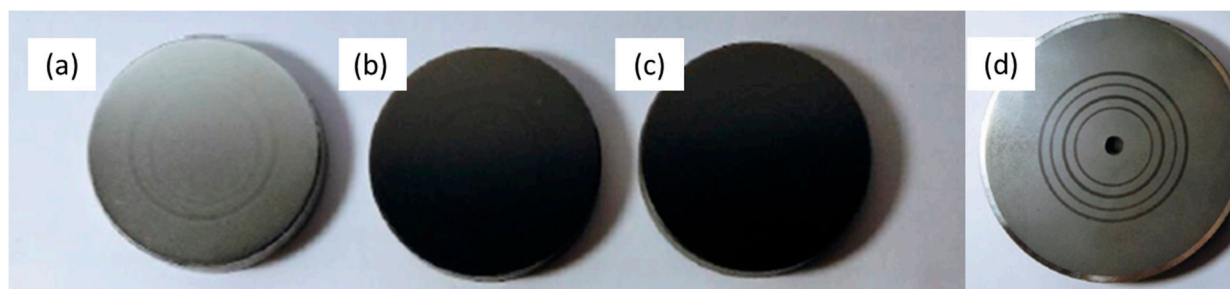


Figure 2. Coatings used for the wear tests: CrN/NbN multi-layer (a), DLC (as deposited) (b), DLC (post-finished) (c), Cr₂O₃ (d).

Table 3. Coated counterparts used in this study.

Coating	Deposition Process	Hardness	Substrate Material	Post Finishing Treatments
CrN/NbN multi-layer	PVD	2300–2700 HV ^a	M2 tool steel	Manual polishing
DLC	PECVD	1800–2400 HV ^a	M2 tool steel	None
				Manual polishing
Cr ₂ O ₃	Atmospheric plasma spraying	844 ± 34 HV _{0.3} ^b	AISI 304 stainless steel	Grinding + polishing

^a Nominal value from the manufacturer. ^b Experimentally measured, from [27].

The CrN/NbN multi-layer coating consisted of alternating nanometer-thin layers of CrN and NbN deposited by cathodic arc evaporation–physical vapor deposition (CAE–PVD). The DLC coating was deposited by plasma-enhanced–chemical vapor deposition (PE–CVD) onto intermediate layers obtained by magnetron sputtering (MS)–PVD to enhance adhesion and provide mechanical support. The CrN/NbN multi-layer coating was manually polished with a 4000 mesh SiC paper to remove the protruding “droplets” (or “macros”) that are typically generated by CAE–PVD processes [39,40]. This prevents unwanted abrasion on the polymer. The DLC coating, which should have fewer defects than the superlattice due to the MS–PVD process for depositing the interlayers, was used both in as-deposited conditions and after manual polishing. Cr₂O₃ was deposited by atmospheric plasma spraying and was ground and polished by the manufacturer.

Different substrate materials were used for the thin-film layers (DLC and CrN/NbN) and the thick Cr₂O₃ coating (Table 3). The thin-film layers need mechanical support from the substrate, so a tool steel was selected, as the film is unlikely to spall off such a hard surface during service [41–43]. Although under the test conditions described in Section 2.2, spallation is unlikely even with a softer substrate, its occurrence would have seriously altered the results of the test. As our aim was not to examine the adhesion/cohesion and service limits of the coatings but the tribological response of the polymer-based materials when coupled with them, this choice ensured that the results were significant. The Cr₂O₃ coating was thick enough for the contact stress distribution to fall entirely within the layer, and thus the substrate material was irrelevant to the outcome of our experiment.

The microstructure of the superlattice and DLC coatings was characterized using SEM (Nova NanoSEM 450, FEI ThermoFisher Scientific, Hillsboro, OR, USA) on cryogenic fracture surfaces, and that of the Cr₂O₃ coating was characterized in [27]. The microstructure of the PTFE composite was characterized using polished cross-sections, which were mounted in cold-setting epoxy resin, cut with a diamond saw, ground with SiC papers (up to 2500 mesh), and polished with a 3 μm polycrystalline diamond slurry and an alumina slurry.

The surface roughness of all coatings was assessed by optical profilometry using a structured-light detector (ConfoSurf, ConfoVis GmbH, Jena, Germany) mounted onto a Nikon Eclipse LV150N microscope operated with a 50× objective. Four measures were performed on each surface, thus acquiring 0.6 × 0.6 mm² surface areas. Surface-related

topographical parameters were extracted according to the definitions in ISO 25148-2, including the arithmetic average surface roughness (S_a), the skewness of the height distribution (S_{sk}), the maximum height of the peaks (S_p), the maximum height of the valleys (S_v), and the maximum height of the surface (S_z).

2.2. Pin-on-Disc Sliding Wear Tests

Tests were carried out at room temperature (≈ 23 °C) using a pin-on-disc tribometer (TRB, Anton Paar—Tritec, Corcelles, CH). The non-conformal contact of the spherically tipped pin (Figure 1) on the disc effectively mimics the non-conformal contact of a lip seal against its counterpart in a simplified test configuration. Four test conditions were used for each pin/disc pair, by combining normal loads of 3 N and 10 N and sliding speeds of 14 cm/s and 54 cm/s. The operating conditions were based on those of ATP S.p.A. and included gaskets typical of those used in filling machines in the food and beverage sector. The sliding distance was 3000 m and the track radius 10 mm in all cases (note that some of the discs in Figure 2 showed multiple wear tracks at different radii, as they were used in preliminary tests to identify a suitable sliding distance).

The diameter of the worn surface of the pin was measured after the test with an optical microscope, and the volume of the worn cap was calculated through geometrical relations.

Data were converted to the specific wear rate, expressed in units of $\text{mm}^3/(\text{N}\cdot\text{m})$, by normalizing over the sliding distance and the applied normal load.

The friction coefficient (μ) was calculated as the ratio between the tangential force acting on the pin during the test, as measured through a load cell, and the normal force applied to the pin itself:

$$\mu = \frac{F_T}{F_N}$$

where F_T is the tangential force measured through a load cell and F_N is the normal acting on the pin.

The two types of scanning electron microscopes used were an environmental scanning electron microscope (ESEM, model: Quanta-200, FEI ThermoFisher Scientific Eindhoven, NL) for worn pin surfaces and debris operated with a water vapor atmosphere at a pressure of 40 Pa, and a scanning microscope with a field-effect emission source (FEG-SEM, model: Nova NanoSEM 450, FEI ThermoFisher Scientific) for the wear traces on the discs. Each was equipped with an energy dispersive X-ray (EDX) detector (INCA, Oxford Instruments Analytical, Abingdon, UK; and Quantax-200, Bruker Nano GmbH, Berlin, Germany, respectively).

The worn and pristine surfaces of the pins were further characterized by Fourier Transform–Infrared Spectroscopy (FT-IR: Vertex 70, Bruker Scientific LLC, Billerica, MA, USA) operated in attenuated total reflection (ATR) mode.

The workflow of the experiment is illustrated by the block diagram in Figure 3.

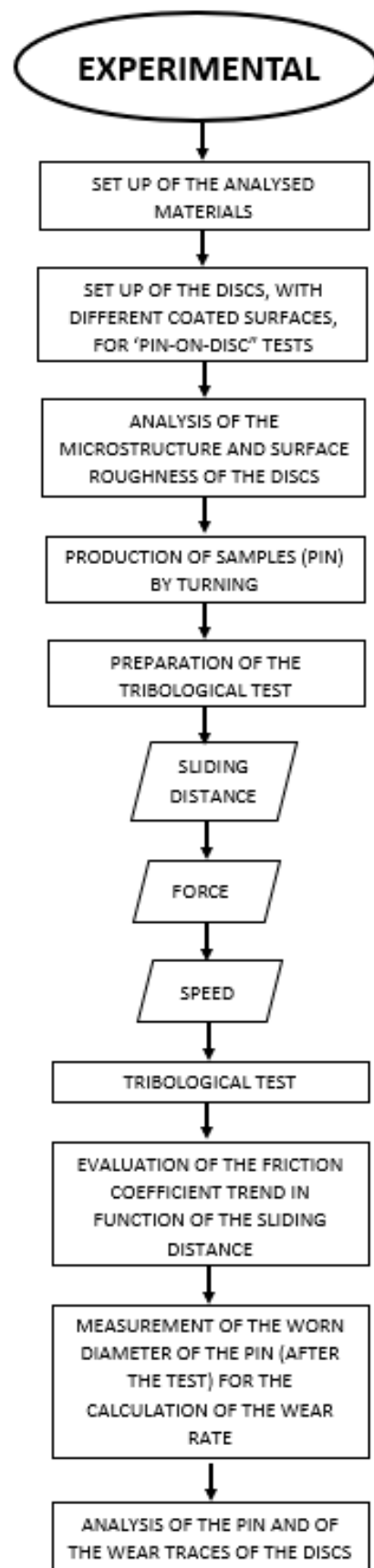


Figure 3. Block diagram of the experimental workflow.

3. Results and Discussion

3.1. Microstructure and Topography of Pins and Countersurface Materials

As mentioned, the approximately 200 μm -thick microstructure of the Cr_2O_3 coating was characterized in [27]. This coating had micron-sized pores and submicron-sized microcracks, which are typical of the plasma spraying process. The grinding and polishing processes resulted in the pores being open to the surface.

The DLC-based and CrN/NbN films were both approximately 3 μm thick (Figure 4A,C). The DLC-based film consisted of several stacked layers. The backscattered electron micrograph shown in Figure 4B and the EDX spectra (not shown in the paper) suggests that the system consisted of a Cr adhesion layer directly deposited onto the substrate (Figure 4B—label 1), followed by a W-Cr-C mixed layer (label 2), a bright W-based layer (label 3), and a relatively thick WC/C interlayer (label 4: note that it has a slightly darker shade compared to layer n. 3). A pure DLC top layer lay on the CrN/NbN film (label 5). The outer surface of the film was smooth but contained occasional clusters (Figure 4A: arrow).

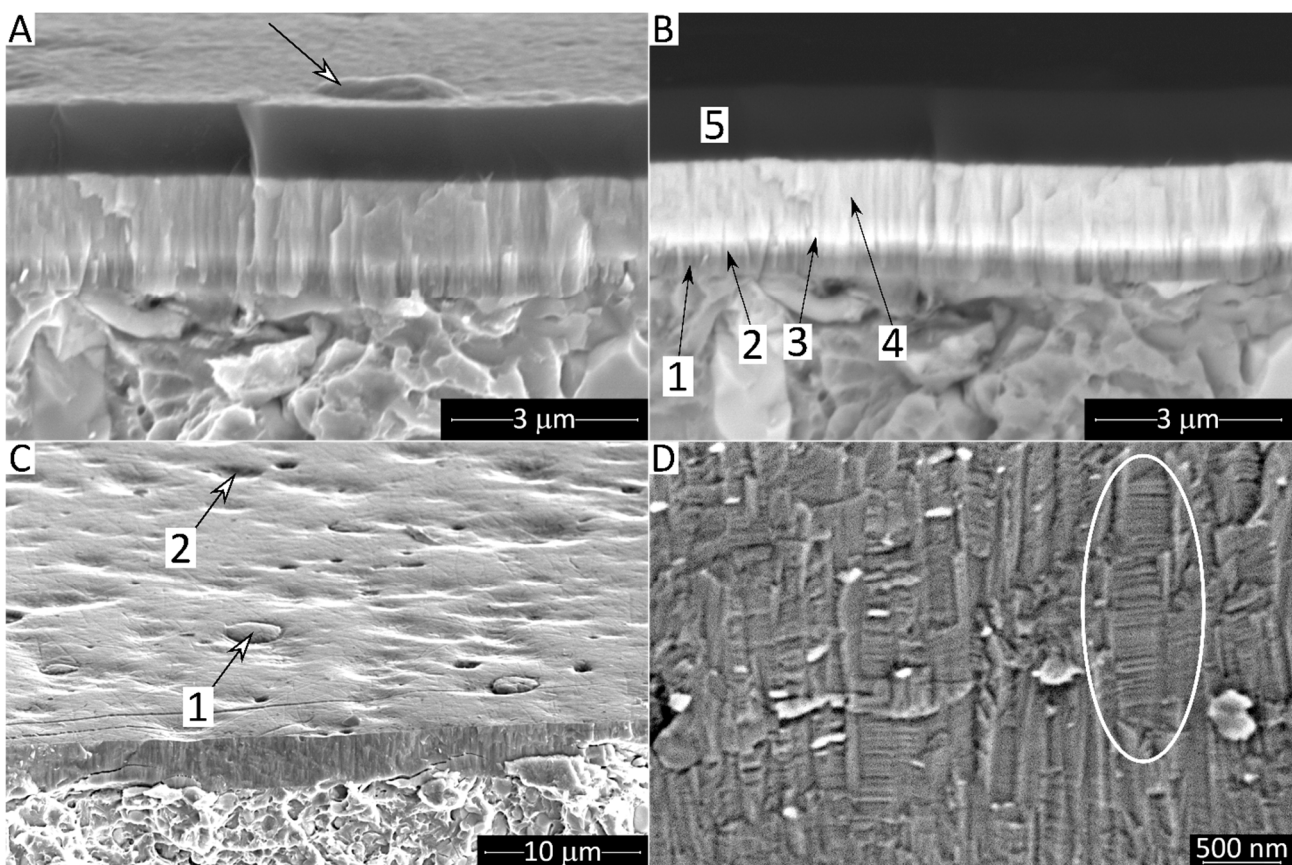


Figure 4. SEM micrographs showing the fracture sections of the as-deposited DLC-based film (A: secondary electrons, B: backscattered electrons) and then manually polished CrN/NbN multi-layer (C: secondary electrons overview; D: backscattered electron detail). The arrow in panel A shows a cluster on the surface; the circle in panel D highlights the visible stacking of CrN and NbN nanometer-thin layers; labels 1–5 in panel B indicate the various layers the DLC-based film was composed of (see the text for a description) and labels 1 and 2 in panel C indicate a smoothed droplet and a pulled-out droplet, respectively.

We confirmed that the CrN/NbN coating consisted of extremely thin layers (Figure 4D: for example, individual layers are distinguishable in the circled area). The microstructure of this type of coating is further discussed in [44–47], for example. Columnar grains grew epitaxially across the entire film throughout the layers (Figure 4C,D). Polishing left slight grooves on the outer surface (Figure 4C), and either flattened down (Figure 4C—label 1) or

more frequently pulled out the “droplets”, which resulted in several small depressions on the surface of the film (label 2).

Consistent with these observations, the profile of the CrN/NbN coating was characterized by a slightly higher average amplitude than both DLC surfaces (Sa, Table 4) but a negatively skewed height distribution (Ssk, Table 4), indicating that the surface had no prominent peaks ($Sp < 1 \mu\text{m}$, Table 4) but rather deeper valleys ($Sv \approx 3 \mu\text{m}$, Table 4).

Table 4. Topography data measured on countersurface materials.

Sample	CrN/NbN Multi-Layer	DLC as Deposited	DLC Polished	Cr ₂ O ₃
Sa [μm]	0.07 ± 0.01	0.02 ± 0.01	0.02 ± 0.01	0.14 ± 0.02
Ssk [μm]	-6.38 ± 1.68	-5.15 ± 22.98	-20.40 ± 8.20	-4.55 ± 0.13
Sp [μm]	0.88 ± 0.13	1.95 ± 0.67	1.15 ± 0.26	0.59 ± 0.07
Sv [μm]	2.92 ± 0.81	2.28 ± 1.32	2.90 ± 0.09	3.79 ± 0.01
Sz [μm]	3.80 ± 0.95	4.22 ± 0.65	4.05 ± 0.16	4.38 ± 0.06

The as-deposited DLC coating had the same Sa value as the polished sample, as clusters, such as that in Figure 4A, were not frequent enough to perceptibly alter the average values. However, the skewness of the height distribution (Ssk) on the as-deposited surface was extremely variable, and changes from negative to positive values depending on whether any cluster was present in the measurement area. The Sp value was thus somewhat higher, and also had a relatively large associated standard deviation. After polishing, the Ssk shifted to consistently negative values and lower and more repeatable Sp values, as the few clusters were removed.

The Cr₂O₃ coating had the highest average roughness (Sa, Table 4), mainly due to the presence of deep valleys, i.e., the micron-sized pores of plasma sprayed coating, as noted at the beginning of this section. The Sp value was even lower than that of the thin-film layers. Accordingly, the height distribution was negatively skewed.

The microstructure of the PTFE-based Syntek 439 composite was verified using SEM. A somewhat homogenous distribution of randomly oriented short glass fibers was recognizable (Figure 5—label 1) together with lamellar h-BN particles (label 2) of a few tens of micrometers in width.

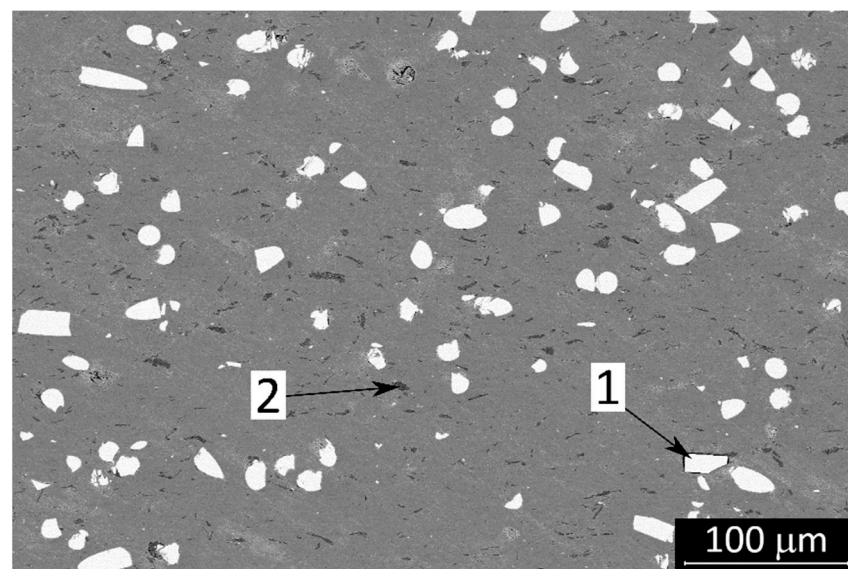


Figure 5. Cross-sectional SEM micrograph (backscattered electrons) of the Syntek 439 PTFE-based composite. Label 1 = glass fiber, 2 = h-BN particle.

The surface profile of each polymeric pin was obtained (see the example in Figure 6) to calculate the exact value of the curvature radius of the spherical cap, which can provide a more precise calculation of the specific wear rate. No radius differed from the nominal 2 mm-value (Section 2.1) by more than a few tenths of a millimeter.

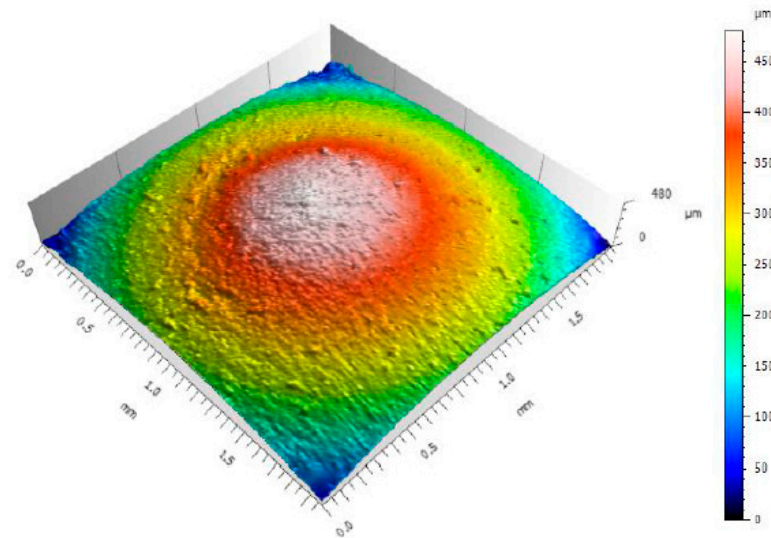


Figure 6. 3D profilometry of the spherical cap of a Syntek PKE pin.

3.2. Sliding Wear Behaviour

3.2.1. Syntek 439

Friction Trends and Specific Wear Rates

The coefficients of friction for Syntek 439 against the thin-film coatings, i.e., the polished CrN/NbN multi-layer (Figure 7B) and the DLC coating, both as-deposited (Figure 7C) and post-finished (Figure 7D) decreased at the beginning of each test and achieved a steady-state regime with a minimum value of around 0.15. However, the steady-state was not maintained throughout the test duration. The distance could change from a few 100 meters to slightly over 2000 m depending on the test conditions and the counterface, and accordingly, the coefficient of friction rose almost monotonically, up to values >0.3 . The steady, low-friction state was maintained longer when against the DLC counterface than when against CrN/NbN, and under conditions of high load and/or high speed. In the test with CrN/NbN at 3 N and 14 cm/s, the coefficient of friction rose after just 200 m (Figure 7B). It increased earlier with a low sliding speed and slightly later under high load/high speed (Figure 7C,D) when against the DLC counterpart (both as-deposited and polished).

The trend of the friction coefficient against Cr₂O₃ (Figure 7A) was remarkably different. A steady-state with a friction coefficient typically between 0.15 and 0.20 (the test at 10 N load and 54 cm/s speed being the only partial exception) was attained almost immediately by the system, and it retained this friction level throughout the test.

A marked difference between the behavior of the PTFE-based pins against different counterparts also emerged in their specific wear rates (Figure 8A). All thin-film counterfaces exhibited similar rates of roughly between 1×10^{-6} and 5×10^{-6} mm³/(N·m), with limited sensitivity to test conditions, although a slight tendency to higher wear rates was observed with increasing load against the CrN/NbN coating and with decreasing load for both types of DLC. In contrast, combining Syntek 439 with the plasma sprayed Cr₂O₃ coating produced much lower wear rates of $1\text{--}2 \times 10^{-7}$ mm³/(N·m), again independent of test conditions.

Analysis and Discussion of Wear Mechanisms

We analyzed the wear mechanisms and identified worn pins, counterfaces, and debris, to assess what led to the differences in behavior.

The debris released by Syntek 439 sliding against the thin-film coated discs contained large agglomerates of up to 1 mm in size (Figures 9A,B,D and 10C), with evidence of extensive plastic deformation and elongation in the sliding direction (see Figure 9B,C in particular). Some of these large agglomerates were more densely compacted and had higher levels of the polymeric constituent (e.g., Figure 9B), while others were observed to consist of more loosely aggregated fragments at micrometric or sub-micrometric sizes, as shown in Figure 10B,C. The corresponding EDX spectra (Figures 9D and 10D) exhibited peaks of Si, Al, Ca, and O in addition to C and F, signaling the presence of fragments from the glass fibers. The thin-film coatings may also have become slightly worn, as Nb and Cr were found in the EDX spectra of the debris produced after sliding against the CrN/NbN counterface (Figure 10D, spectra 1 and 2). Ascertaining whether there was debris from the DLC coating in the corresponding debris (Figure 9D) was impossible because DLC consisted of pure C, and thus it could be confused with C from the PTFE, from the adhesive tab, or with adventitious carbon from unavoidable environmental contamination.

In addition, the debris contained smaller lumps (Figure 10A), which provide clear evidence of plastic deformation.

Correspondingly, at high magnifications, the worn pin surfaces clearly showed evidence of plastic flow in the PTFE matrix (Figure 11B,D). Morphological features resembling small lumps, such as those in Figure 9A, could be observed to be about to come off. At lower magnifications (Figure 11A,C), abrasive grooves were observed in the matrix (label 1). Glass fibers (label 3) with a smooth surface that indicated mild polishing wear protruded out of the surface, and debris (label 2) were accumulated against the protruding fibers. The composition of the debris was the same as that observed in the previous EDX spectra.

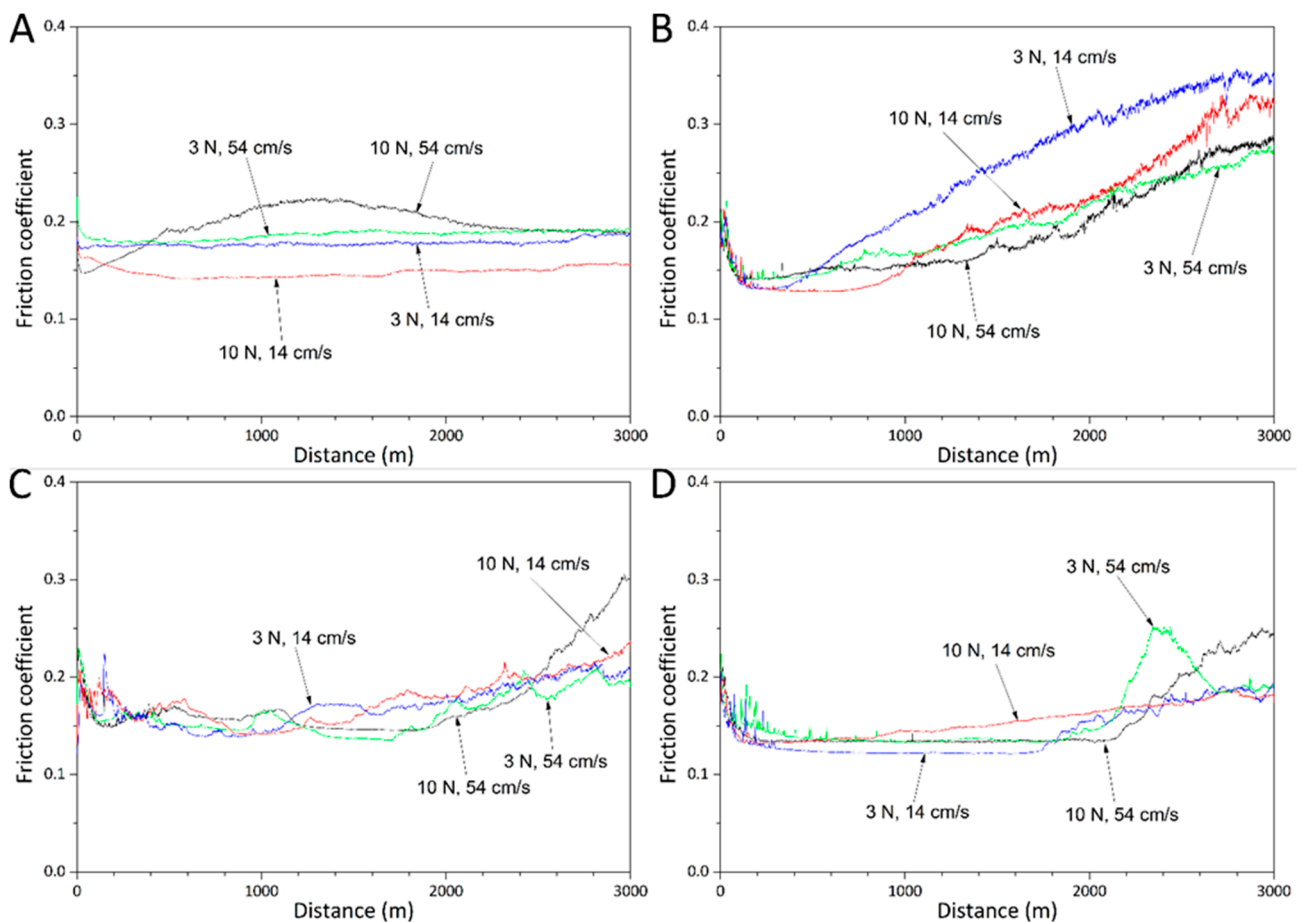


Figure 7. Friction curves for the PTFE-based composite tested against Cr₂O₃ (A), CrN/NbN (B), DLC in as-deposited condition (C), and polished DLC (D).

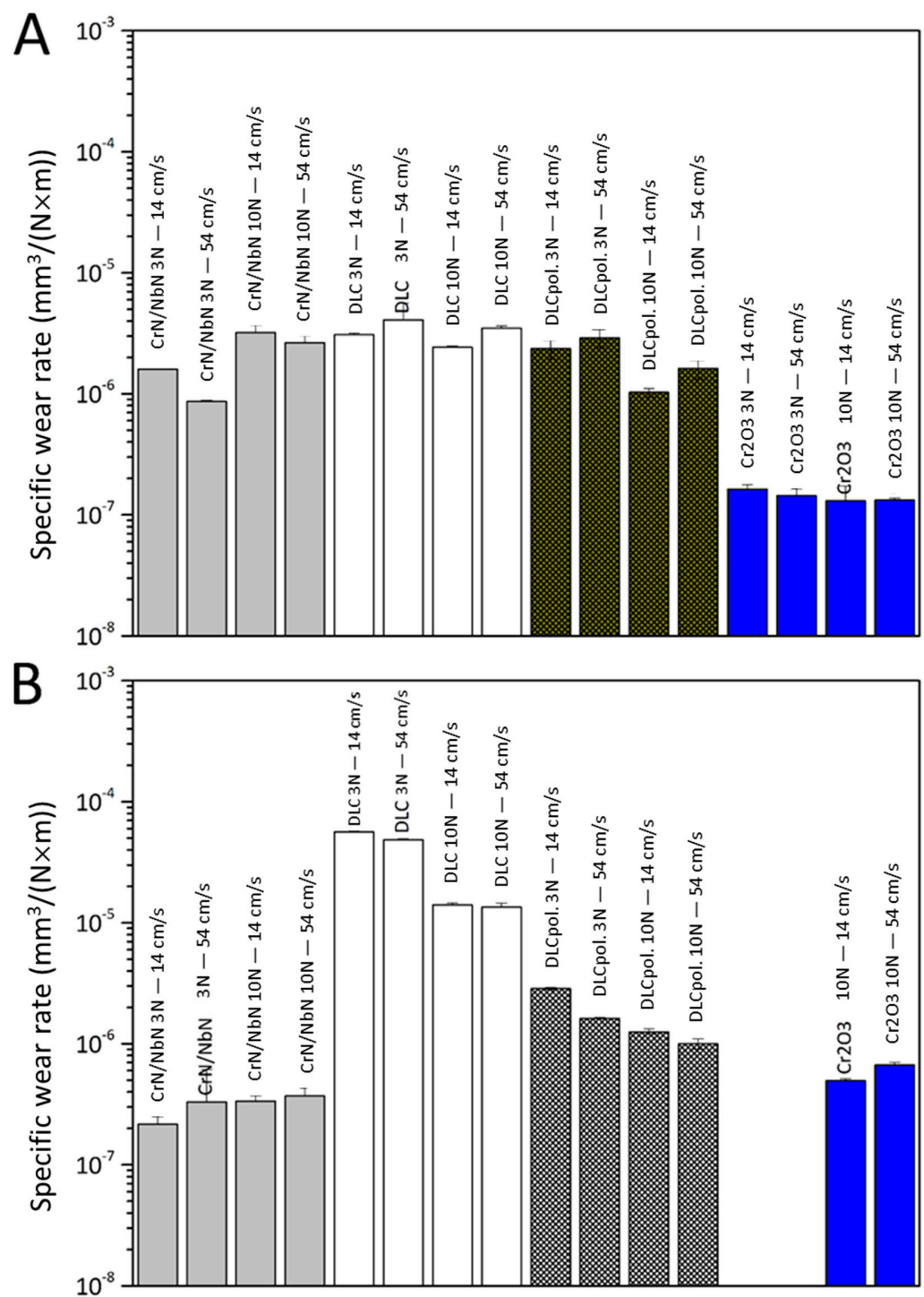


Figure 8. Specific wear rates of the polymeric pins after pin-on-disc sliding wear tests—PTFE-based Syntek 439 (A) and polyketone (B). The counterface and test conditions (normal load, sliding speed) are specified on top of each column.

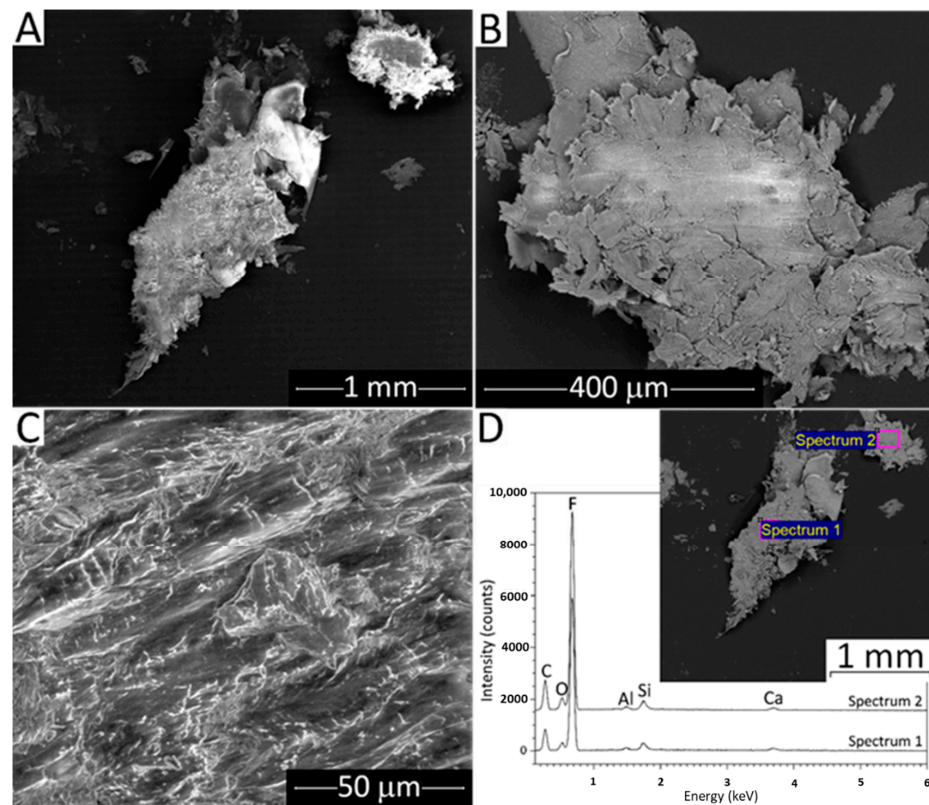


Figure 9. SEM micrographs of debris particles collected after testing the Syntek 439 PTFE-based pin against the as-deposited DLC coating at 10 N load, 54 cm/s speed (A,B: overviews, C: detail), and corresponding EDX spectra (D).

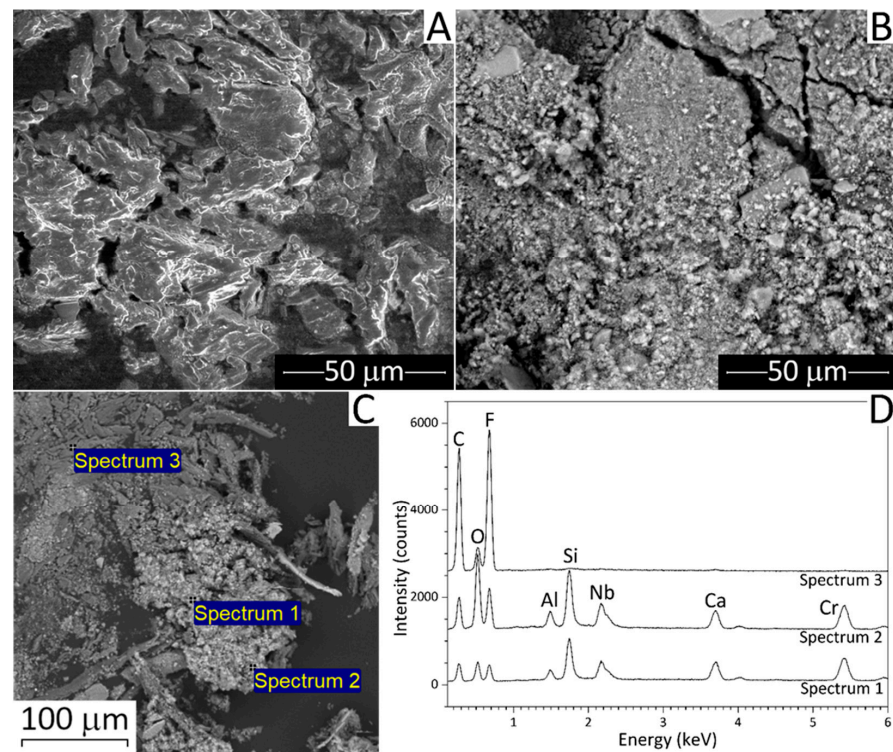


Figure 10. SEM micrographs of debris particles collected after testing the Syntek 439 PTFE-based pin against the polished CrN/NbN coating at 10 N load, 54 cm/s speed (A–C), and corresponding EDX spectra (D).

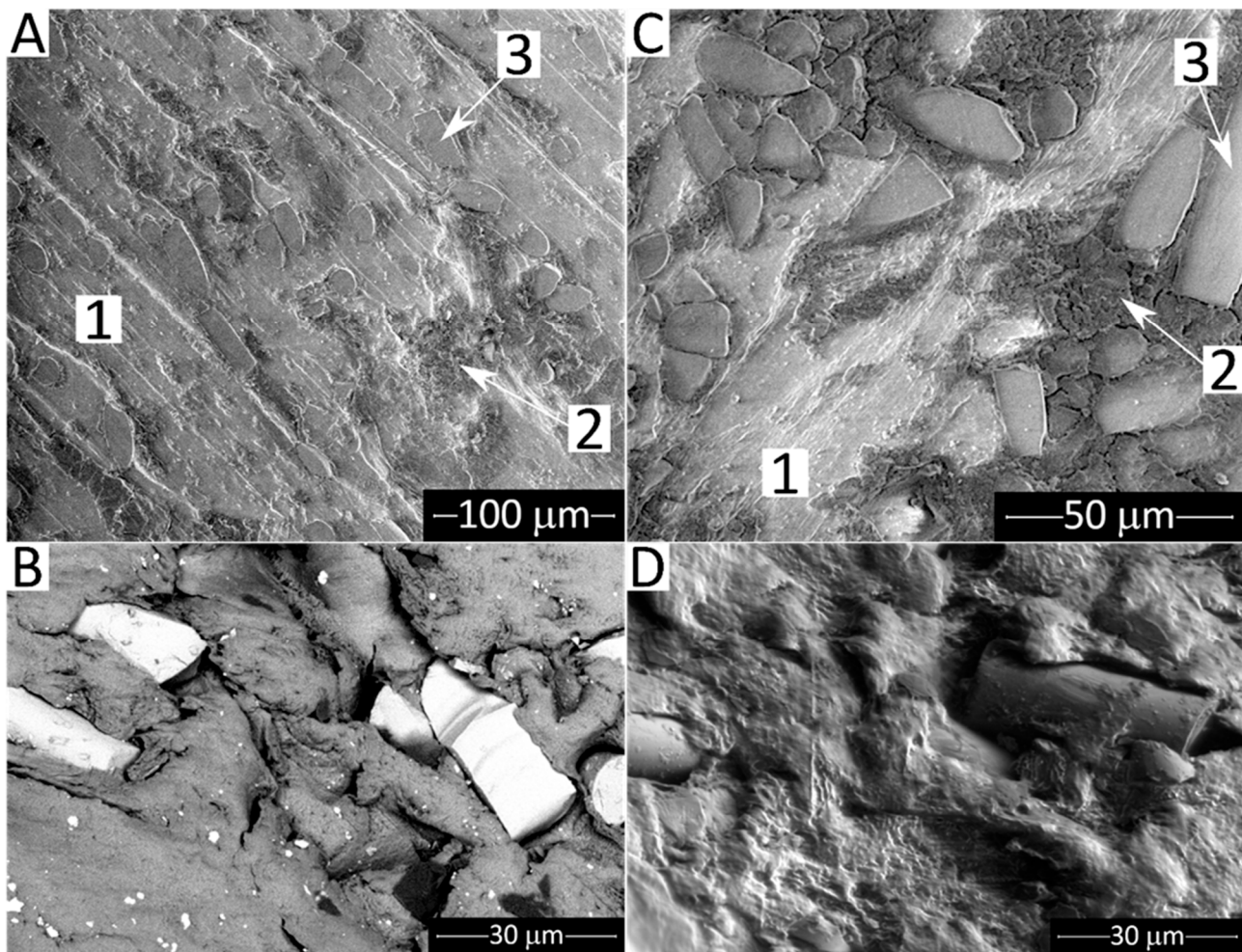


Figure 11. SEM micrographs of the worn surfaces of the Syntek 439 PTFE-based pin after testing against the polished CrN/NbN coating at 10 N load, 54 cm/s speed (**A,B**), and against the as-deposited DLC coating (**C**: 10 N load, 54 cm/s speed; **D**: 3 N load, 54 cm/s speed). Label 1 = PTFE matrix, 2 = debris, 3 = glass fiber.

The cross-sectional views in Figure 12 confirm that debris accumulated on the pin surface and showed how it formed into a thin tribo-layer (Figure 12A: white arrows). As for the loose debris in Figures 9D and 10B,C, the tribo-layer was a compaction of fine particles (see the detail in Figure 12B), together with somewhat bigger fragments of glass fibers (label 1). The debris included h-BN particles (label 2), which could not be clearly discerned in the previous micrographs but were clearly visible on a metallographically polished sample

The composition of the tribofilm can be further investigated through FT-IR spectroscopy (Figure 13). Identifying the difference between the spectrum acquired on the worn surface and that of the unworn material can determine any variation. Although changes in the intensity of the peaks associated with the different vibration modes of CF_2 units at 1200 cm^{-1} , 1145 cm^{-1} , 638 cm^{-1} , and 625 cm^{-1} [48] were not meaningful (they can depend on how well distinct samples can be pressed against the ATR crystal), the difference spectrum highlighted the appearance of new, although weak, absorption bands on the worn surface. The band between 3000 and 3600 cm^{-1} was probably due to adsorbed water and hydroxyl groups [49,50]; that at 1650 cm^{-1} might belong to carbonyl groups and/or to hydroxyl groups [49]; and the broad band approximately located between 1100 cm^{-1} and 850 cm^{-1} might result from the overlapping of signals from Si-O-Si and Si-O⁻ units [49–51] and C-H and C=C units.

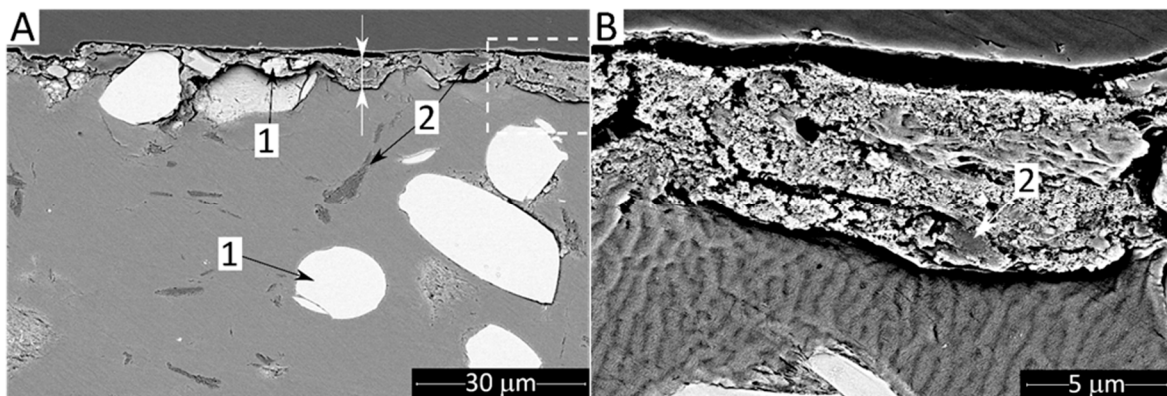


Figure 12. SEM micrographs of the polished cross-section of the Syntek 439 PTFE-based pin after wear testing against the polished CrN/NbN coating at 3 N load, 14 cm/s speed (**A**: overview, **B**: detail of the dashed area in panel **A**). Label 1 = glass fiber, 2 = h-BN particle; white arrow = debris tribo-layer.

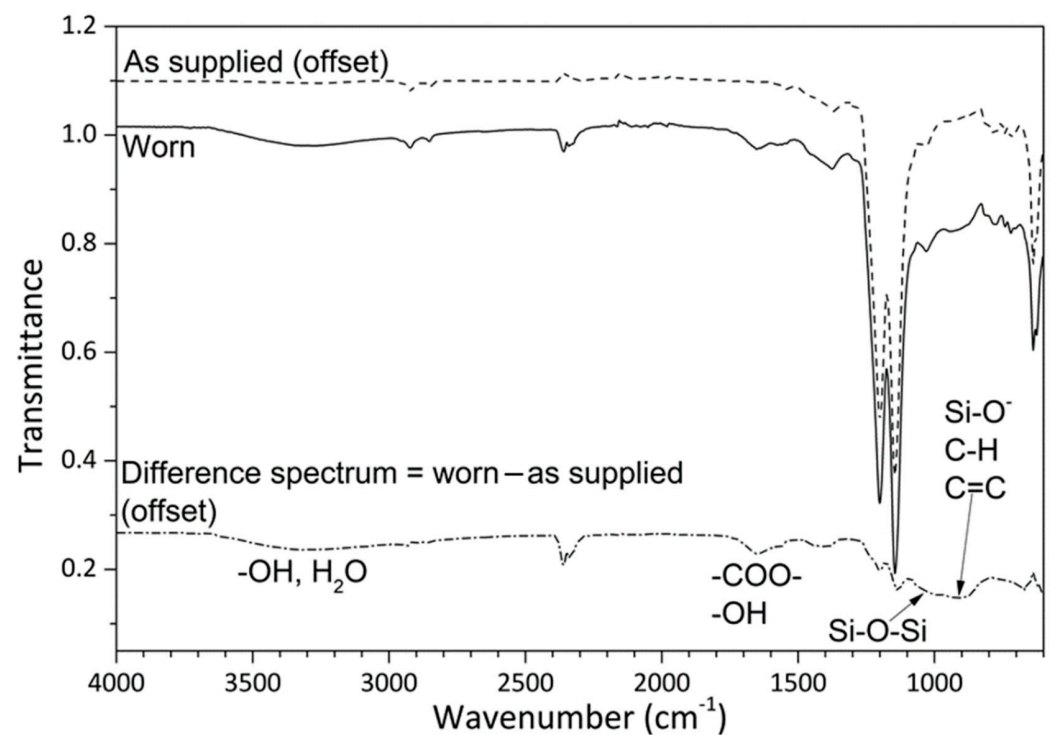


Figure 13. FTIR spectra of an as-supplied Syntek 439 PTFE-based composite, a worn surface of the same pin after ball-on-disc testing against the CrN/NbN coating at 10 N load, 54 cm/s speed, and the difference between the two spectra. Spectra were offset vertically for improved readability.

The debris layer on the worn surface of the pin results in these changes, and these new absorption bands were more distinct when the worn surface exhibited greater tribo-layer coverage (i.e., when tested against CrN/NbN) and less distinct with less coverage. This confirms that the debris layer contained silicate glass fragments and that the PTFE polymer experienced minor chemical degradation (the formation of -COO- and probably C-H and C=C bonds). Molecular water and hydroxyl groups were probably adsorbed from environmental humidity, due to the hydrophilic nature of the glass debris and the formation of polar groups (-COO-) on tribo-chemically altered PTFE.

Based on this evidence, the wear mechanisms of the Syntek 439 composite, as tested against CrN/NbN and DLC coatings, can be described as follows. The PTFE matrix underwent adhesive and some abrasive wear. Both mechanisms were characteristic of PTFE-based materials [52]. Adhesive wear was manifested through the detachment of small, plastically

deformed lumps of material. Abrasive wear can be due to asperities on the counterface, which were reduced in the manually polished surfaces but not to zero, and the release of fragments of glass fibers in the debris. The fibers were also mildly abraded or fragmented and pulled out.

The debris that remained in the contact area were plastically deformed and could stick back onto the mating surfaces, forming a PTFE-based tribo-layer that partly covered both the pin and the disc. As discussed, the cohesiveness of the debris was increased by the adsorption of environmental humidity in the form of molecular water and hydroxyl groups. Water and -OH groups promoted hydrogen bonding. Their adsorption was due to the presence of hydrophilic glass particles and the formation of polar groups through the (limited) chemical alteration of the PTFE polymer. The formation of the tribo-layer probably corresponded to the onset of the stable, low-friction regime shown in Figure 7, as has been widely reported for PTFE-based materials [8]. The tribo-layer had low surface energy, as it was based on PTFE (albeit with polar groups and glass particles), and also contained h-BN, which contributed to additional solid lubrication.

We can infer from this assumption that the onset of a high-friction regime in the final stages of the ball-on-disc tests was due to the detachment of the tribo-layer from the thin film-coated discs. Accordingly, very little or almost no tribo-layer covered the sliding traces on the CrN/NbN and DLC coatings at the end of the test (Figure 14A,B), i.e., after friction had already entered the rising stage. The presence of large agglomerates (Figures 9 and 10) also indicated an unstable, poorly adherent tribo-layer. The formation of this type of debris during the sliding wear processes of PTFE-based materials is typically associated with high friction [8], as found in our tests. These large agglomerates were probably not removed directly from the pin, as they were almost as large as the diameter of the wear scar itself. The pin would therefore have suffered very severe wear if such debris were directly removed, which is inconsistent with the relatively mild wear rate values reported in Figure 8A. The worn surfaces of the pins would have also been macroscopically much rougher than shown in Figure 11A,B. The formation of the large agglomerates was the result of a dynamic process involving the continued addition of material released from the mating surfaces, as the tribo-layer did not properly attach.

The chemistry and relatively low roughness of the tribo-layer accounted for its limited adhesion to the thin-film coatings. The cavities on the polished coatings were likely too small to retain the tribo-layer. As noted in the Introduction, a roughness of $R_a \approx 0.2\text{--}0.4\ \mu\text{m}$ is often recommended to maximize the adhesion of a transfer layer. However, this is incompatible with thin, hard coatings, such as DLC or CrN/NbN, because it will result in the localization of contact stresses on brittle asperities and may eventually lead to spallation. However, chemical interactions have also been found to enable the adhesion of PTFE-based transfer films onto a metallic (e.g., steel) counterface. These are due first to the presence of oxide-based debris from reinforcements (such as the glass fibers of the present sample) [6,8]. In addition, tribologically induced chemical alterations of the PTFE molecule (as detected through the FTIR spectra previously discussed) can lead to a series of complex chemical interactions that are not fully understood, which may also involve the formation of metal fluorides [8,13,53–55]. These interactions might not be as effective with DLC and nitride films rather than metallic surfaces, although examining specific surface chemical interactions is out of the scope of this study.

Interestingly, the surface of the as-deposited DLC coating was found to be slightly abraded at the end of the test (Figure 14A), while the polished DLC (Figure 14B) and CrN/NbN films (not shown) did not exhibit the same resulting grooves. The abrasion of the as-deposited DLC surface may be due to the pull-out of some of the pre-existing protrusions (Section 3.1) that act as hard abrasives. The lack of abrasive grooving on the CrN/NbN surface would seem to contradict the presence of Cr and Nb in the corresponding debris, but the Cr and Nb were likely to be primarily from the pull-out of some of these “droplets” that were flattened but not removed during polishing (Section 3.1). As they were primarily made of metal (not of nitrides), they did not exert the same abrasive action as the hard DLC clusters exerted on the corresponding coating.

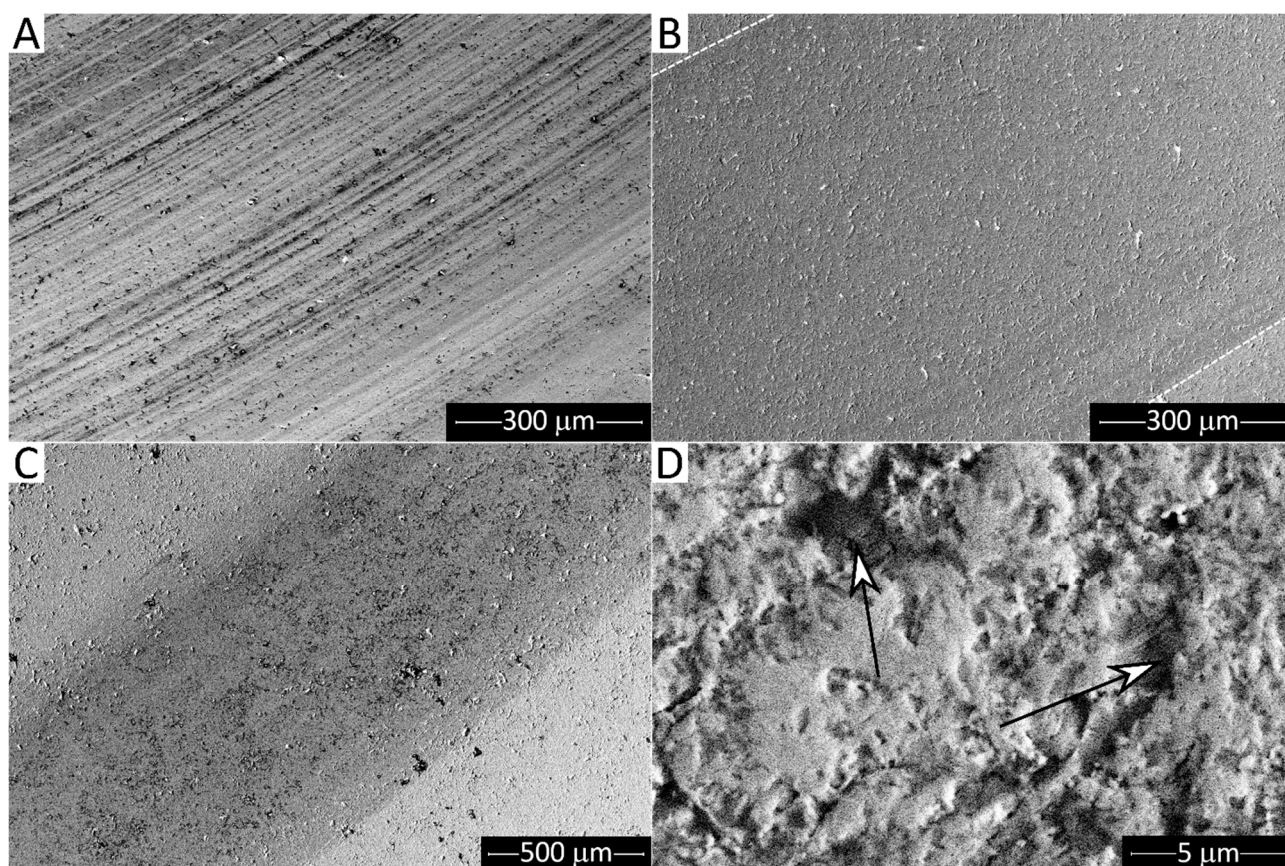


Figure 14. SEM micrographs of the sliding traces on the surfaces of discs after testing against the Syntek 439 PTFE-based composite pins—(A) as-deposited DLC, 10 N load, 14 cm/s speed; (B) polished DLC, 10 N load, 54 cm/s speed; (C,D) Cr₂O₃, 10 N load, 54 cm/s speed. Arrows in the detail of panel D indicate debris residuals embedded in the open pores of the Cr₂O₃ coating.

The tribological behavior on the Cr₂O₃ surface (Figure 14C,D) was markedly different. The Cr₂O₃ counterface generally remained covered by a tribo-layer at the end of the test, which is consistent with the retention of a stable and low friction coefficient throughout the test. The same behavior was previously observed in sliding wear tests with glass fiber-reinforced PTFE (without h-BN) against the same type of counterface [27]. Notably, the friction coefficients recorded in these tests against Cr₂O₃ were lower than those reported in [27], which is presumably due to the additional solid-lubrication effect of h-BN entrained in the debris.

The surface chemistry of an oxide ceramic differed from those of DLC or a nitride-based layer, and Cr₂O₃ also featured numerous dales of varying size, including some that were much larger than those on the thin-film coatings (Section 3.1). This topography facilitated the retention of the tribo-layer, as discussed by the authors in their previous paper [27], and confirmed by the detail in Figure 14D, where the tribo-layer (arrows) appeared to be mainly located in the dales.

The correspondence between tribo-layer retention and stability of the low-friction regime confirmed that the retention or loss of the layer on the counterface is the key to reducing friction, and thus wear.

The worn surface of the pins tested against the Cr₂O₃ coating was accordingly smooth (Figure 15A), and tribochemical wear (in the form of tribo-layer formation) was the dominant mechanism under these conditions. The adhesion of the PTFE matrix to the counterpart became less likely, as the tribo-layer mediates the contact, and thus adhesive wear was greatly reduced. The wear debris, therefore, did not contain either large agglomerates or smaller lumps, but rather curled ribbons and “filings” (Figure 15B), which are indicative

of the abrasive wear of the matrix and likely due to unfilled valleys on the Cr_2O_3 surface, whose sharp boundaries act as a cutting edge. As the results in Figure 8A clearly demonstrated, this type of wear proceeds at a lower rate. As most of the valleys are filled, most did not exhibit sharp, cutting edges after an extremely brief run-in.

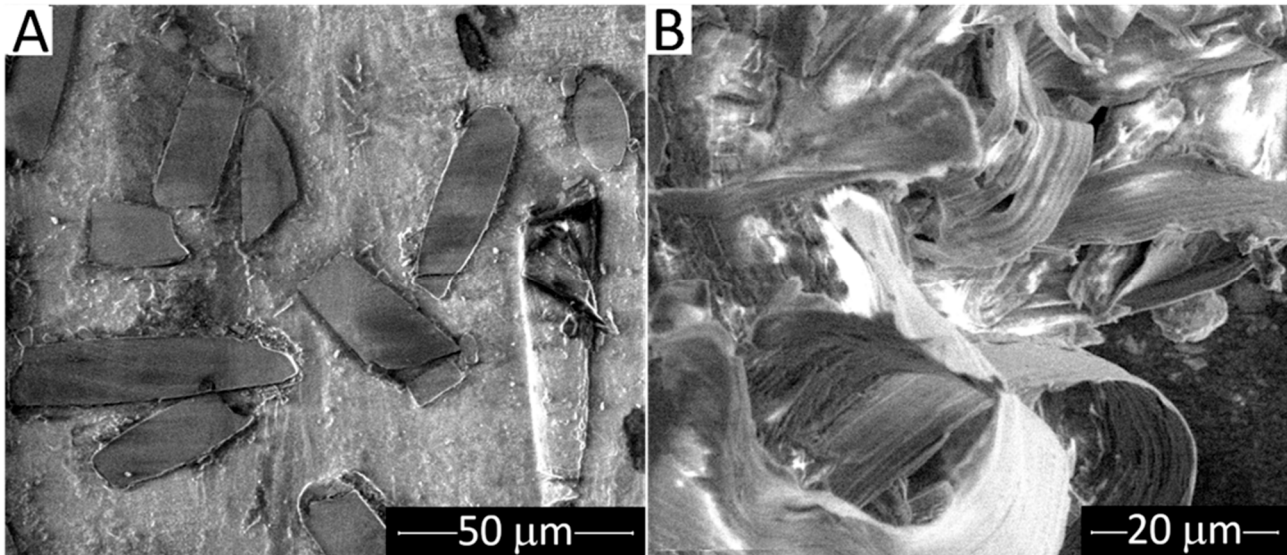


Figure 15. SEM micrographs of the worn surface of the Syntek 439 PTFE-based pin after testing against the Cr_2O_3 coating at 10 N load, 54 cm/s speed (A), and corresponding wear debris (B).

3.2.2. Syntek PKE

Friction Trends and Specific Wear Rates

The polyketone pin consistently produced much higher friction than the PTFE composite, with values between 0.5 and 1.0 (as in Figure 16, which can be compared with those for the PTFE-based pin in Figure 7). This is approximately consistent with the range of friction coefficients recorded in pin-on-disc tests of polyketone against a steel counterface at various pressures and speeds [48]. In all cases, the friction coefficient increased in the early stages of the test and tended to stabilize with increasing sliding distance. The value of the friction coefficient was approximately 0.7 in conditions of high sliding speeds and 0.9–1 in conditions of low sliding speeds. Although with the CrN/NbN counterface the effect of the applied load was clearly visible (lower friction at higher applied load, Figure 16B), this was not the case for the other counterfaces (Figure 16A,C,D). The friction of the polished DLC counterface (Figure 16D) was higher than that in the as-deposited condition (Figure 16C).

In tests involving polyketone pins, lower friction was not associated with lower specific wear rates or vice versa. The as-deposited DLC counterface (see Figure 8B) obtained the highest specific wear rates by far, despite the comparatively lower friction coefficient (Figure 16C), while the tests against CrN/NbN and Cr_2O_3 produced lower pin wear (Figure 8B) although the friction coefficient (Figure 16A) was higher. In addition, although friction decreased with the applied load in tests against CrN/NbN (as noted above), the specific wear rate of polyketone in this tribocouple appeared to be independent of the applied load under the present conditions.

When comparing the wear resistance of the polyketone pin (Figure 8B) to the Syntek 439 PTFE-based composite (Figure 8A), the former exhibited much better wear resistance when coupled with CrN/NbN, comparable performance against polished DLC, slightly higher wear against Cr_2O_3 , and much worse wear resistance against as-deposited DLC. Although the relationship was not perfectly monotonic, it looked like higher specific wear rates occurred with counterfaces having higher S_p values (Table 4). Namely, the wear of the polyketone pin increased as the counterface displayed more prominent protrusions. Accordingly, it was reported [48] that polyketone sliding against a tool steel counterface

with $R_a = 0.11 \mu\text{m}$, which likely possesses some prominent asperities, suffers specific wear rates between $\approx 8 \times 10^{-6} \text{ mm}^3/(\text{N}\cdot\text{m})$ and $4 \times 10^{-5} \text{ mm}^3/(\text{N}\cdot\text{m})$, i.e., higher than were measured against polished counterfaces in this work (Figure 8B).

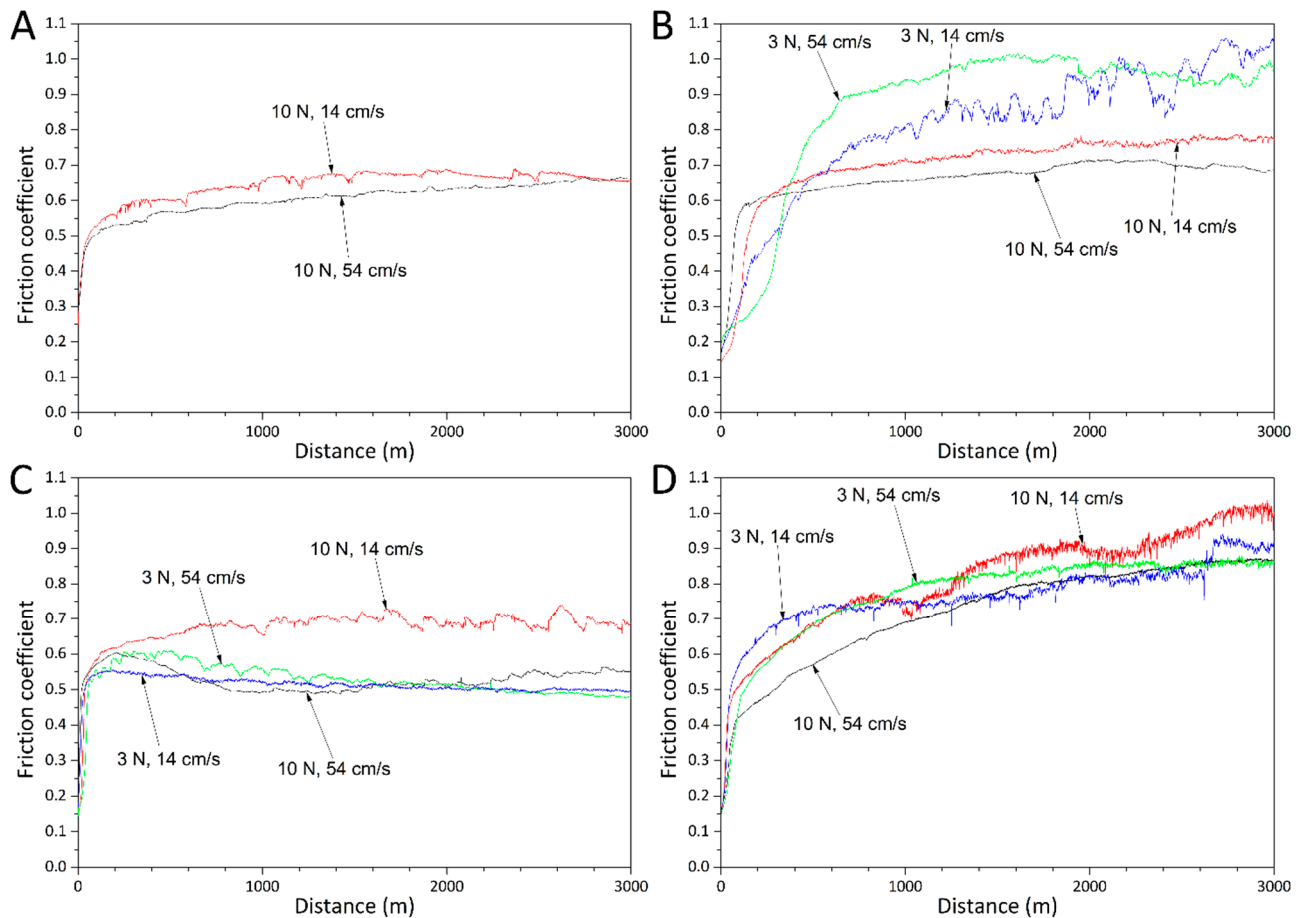


Figure 16. Friction curves for polyketone tested against Cr_2O_3 (A), CrN/NbN (B), DLC in as-deposited condition (C), and polished DLC (D).

Analysis and Discussion of Wear Mechanisms

SEM micrographs of worn surfaces (Figure 17) highlighted that wear of the polyketone composite proceeded through a combination of ductile abrasion, with both sharp grooves suggestive of micro-cutting (label 1) and blunt ones due to micro-plowing (label 2) and adhesion (label 3).

The debris contained curled ribbons due to cutting (Figure 18A—label 1) and blocky or lamellar-shaped lumps, resulting from adhesive/delaminative wear (Figure 18A—label 2). Some of the debris became stuck back onto the worn surfaces (Figure 17A,C,E—label 4). The differences in the specific wear rates recorded for the various counterparts were clearly associated with the specific severity of the mechanisms. In particular, the abrasive grooving became more severe when against surfaces with more prominent asperities, such as the as-deposited DLC (Figure 17C,D).

Both adhesive and abrasive wear were identified in the Syntek 439 PTFE-based composite, but abrasive wear appeared to be much more significant with polyketone, and thus the behavior of this polymer differed from that of the other counterparts. The abrasiveness of the counterface became the main factor controlling the wear of polyketone. For the PTFE-based composite, abrasive wear was mitigated by the presence of the hard reinforcement (glass fibers), and thus tribo-layer retention was the dominant factor.

The transfer of polymer-based material to the counterface also occurred with polyketone (Figure 19). Transferred polymer was found particularly inside the valleys of all the polished

surfaces (Cr_2O_3 : Figure 19G,H; CrN/NbN: Figure 19A,B; polished DLC: Figure 19E,F). The polished DLC and CrN/NbN surfaces appeared to exhibit greater retention of polyketone at the end of the wear test than the PTFE-based composite (compare Figure 19E to Figure 14B). The detection of transferred polyketone on a DLC surface by EDX was not easy, as carbon is the main constituent of both DLC and polyketone, and thus the polyketone residuals in roughness valleys were identified by a stronger oxygen peak (Figure 20A,B: spectra 1 and 3) than that observed on smooth areas (Figure 20A,B: spectrum 2). The retention of transferred polyketone, therefore, appeared to promote a low-wear regime. As discussed in Section 3.2.1—Analysis and Discussion of Wear Mechanisms, filling the valleys with polymer material probably reduced the cutting effects of their hard edges.

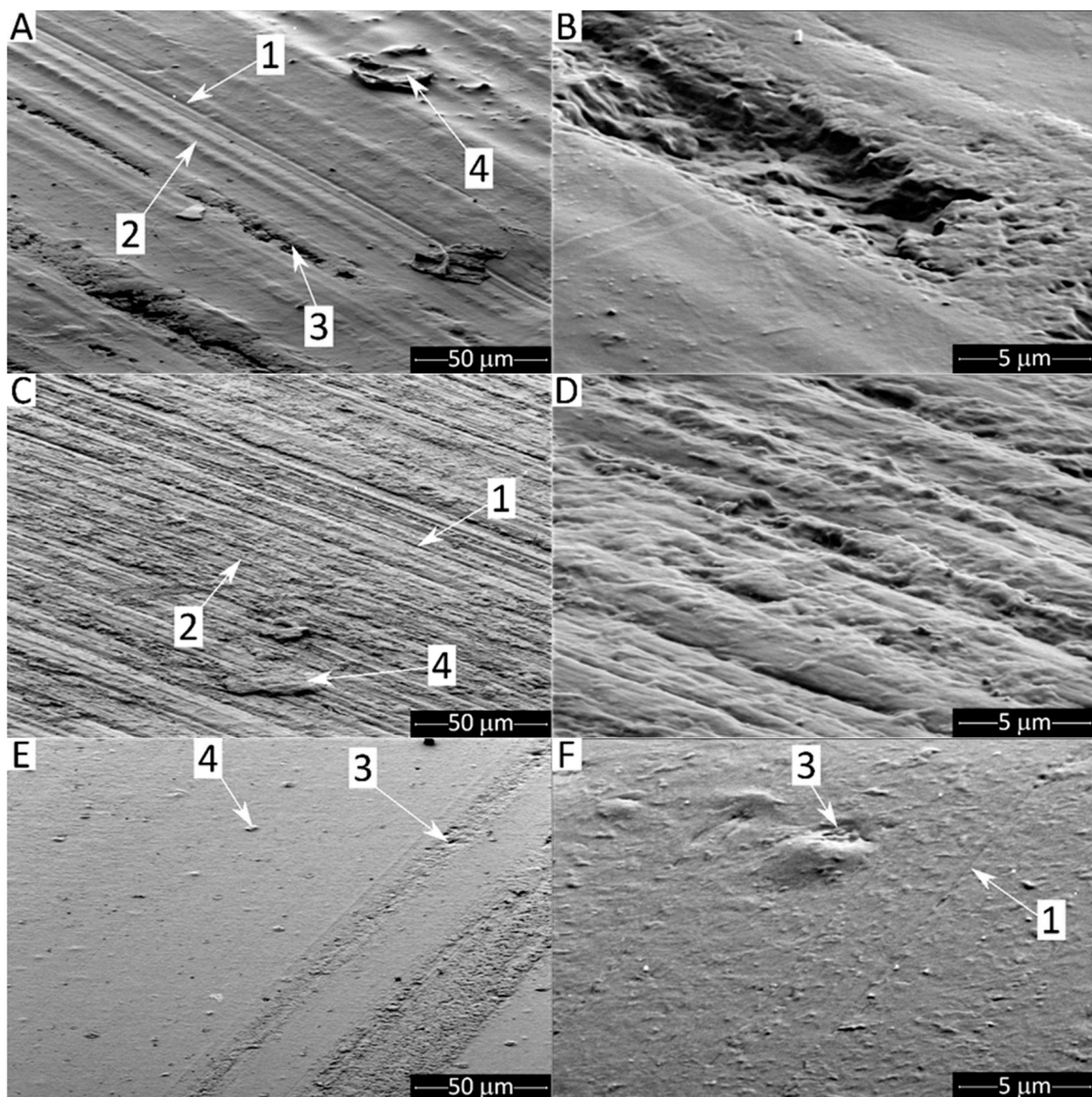


Figure 17. SEM micrographs showing the worn surfaces of polyketone pins after ball-on-disc testing against CrN/NbN (A,B), as-deposited DLC (C,D) and Cr_2O_3 (E,F)—10 N load, 14 cm/s speed. Panels A,C,E = overviews; B,D,F = details. Label 1 = micro-cutting, 2 = micro-plowing, 3 = adhesive wear, 4 = sticking debris particles.

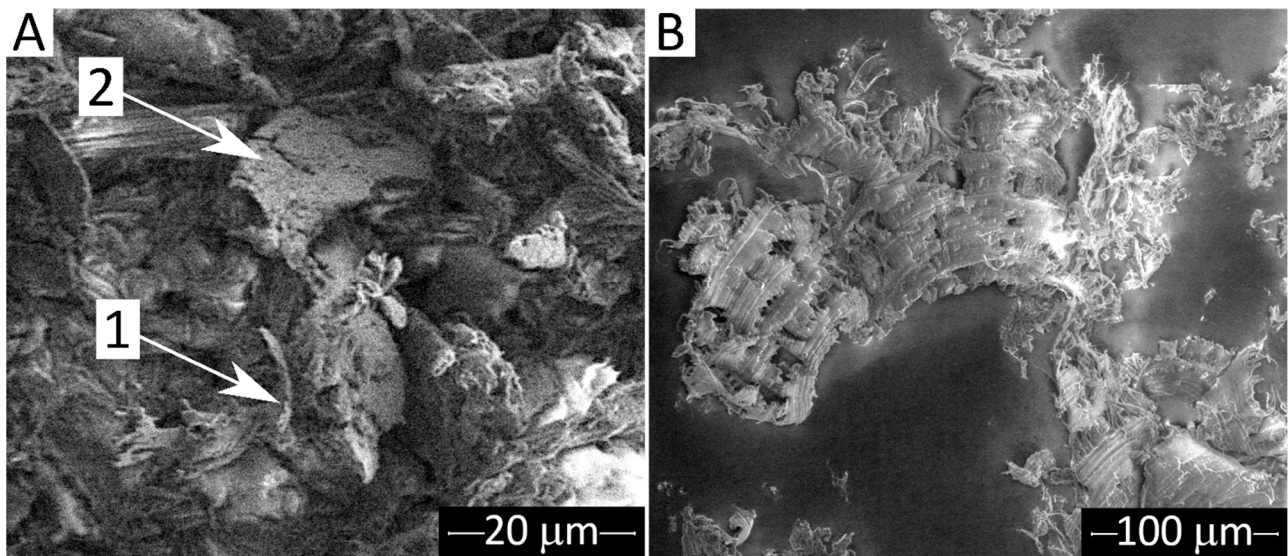


Figure 18. SEM micrographs of wear debris collected after wear testing of polyketone pins against CrN/NbN (A) and Cr₂O₃ (B)—10 N load, 54 cm/s speed.

However, although the formation of a transfer layer was also associated with a low-friction regime for the PTFE-based composite, the presence of transfer material with polyketone appeared to be associated with higher friction. The lowest friction coefficient was recorded against the as-deposited DLC, as the only counter-surface that exhibited almost no retention of transferred polyketone. Figure 19C,D thus show fewer valleys on the as-deposited surface of the DLC coating, which were filled with less debris than the more numerous valleys on the corresponding polished surface (Figure 19E,F). Figure 20C,D confirm that when using the EDX spectra almost no oxygen peak (indicative of the presence of transferred polyketone) was found in valleys (spectrum 1) or smooth areas (spectrum 2) of the as-deposited DLC surface, unlike for the polished DLC surface in Figure 20A,B. Polyketone does not possess the same low surface energy as PTFE, nor does it contain the h-BN particles, which were added to the Syntek 439 composite.

Finally, sliding did not appear to induce any structural change in polyketone, as the FTIR spectrum of the pins remained unaltered after the wear test (Figure 21). The spectra of polyketone matched the nominal values, with a prominent C = O absorption peak at 1689 cm⁻¹, CH₂ vibration peaks in the 2800–3000 cm⁻¹ range, CH₂ wagging and twisting peaks between 1409 cm⁻¹ and 1257 cm⁻¹, a C-C absorption peak at 1057 cm⁻¹, and a skeletal vibration peak at 804 cm⁻¹ [56].

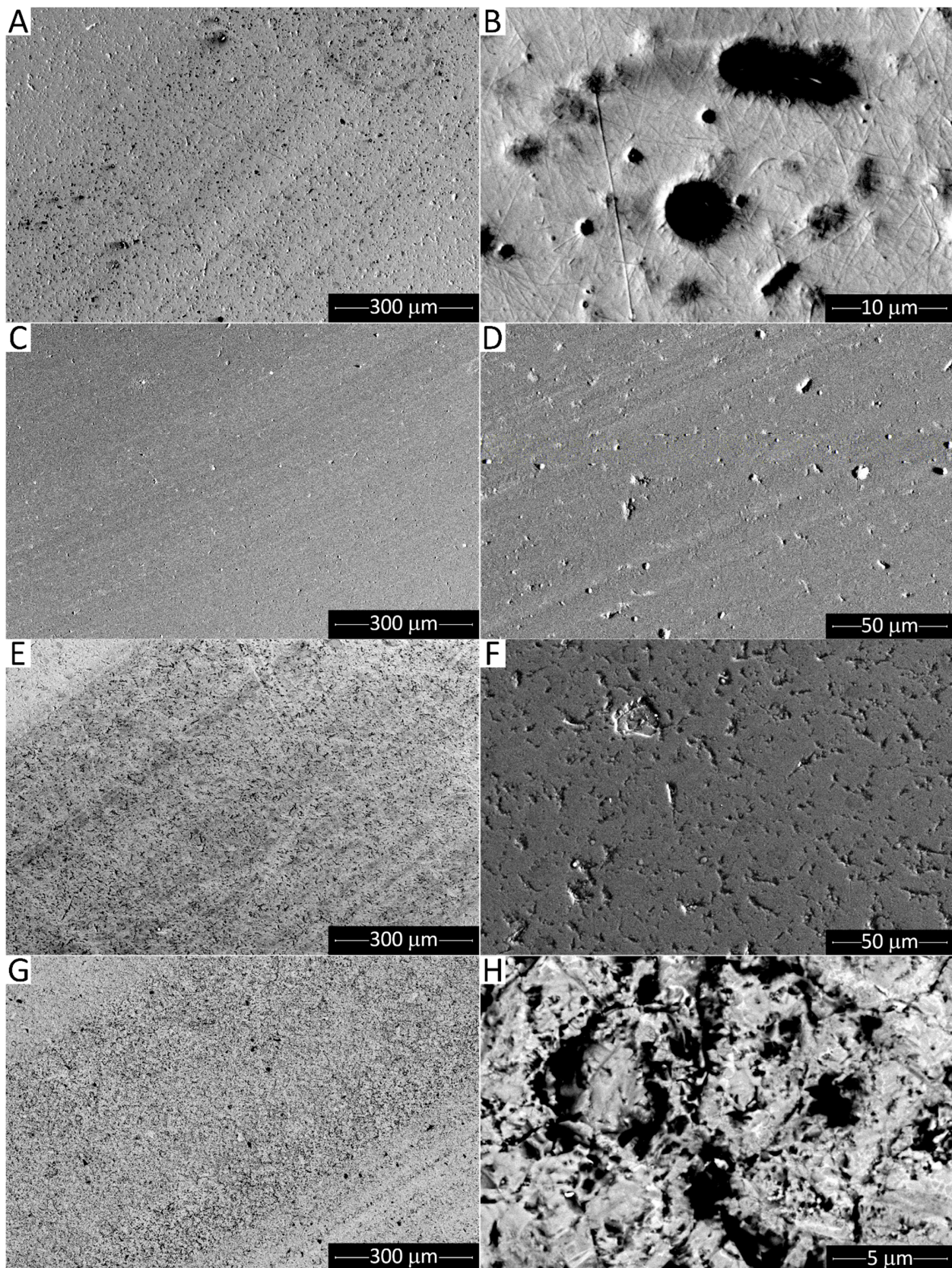


Figure 19. SEM micrographs of the sliding traces on the surfaces of discs after testing against polyketone pins, 10 N load, 54 cm/s speed—(A,B) CrN/NbN, (C,D) as-deposited DLC, (E,F) polished DLC, (G,H) Cr₂O₃. Panels A,C,E,G: overviews; panels C,D,F,G: details.

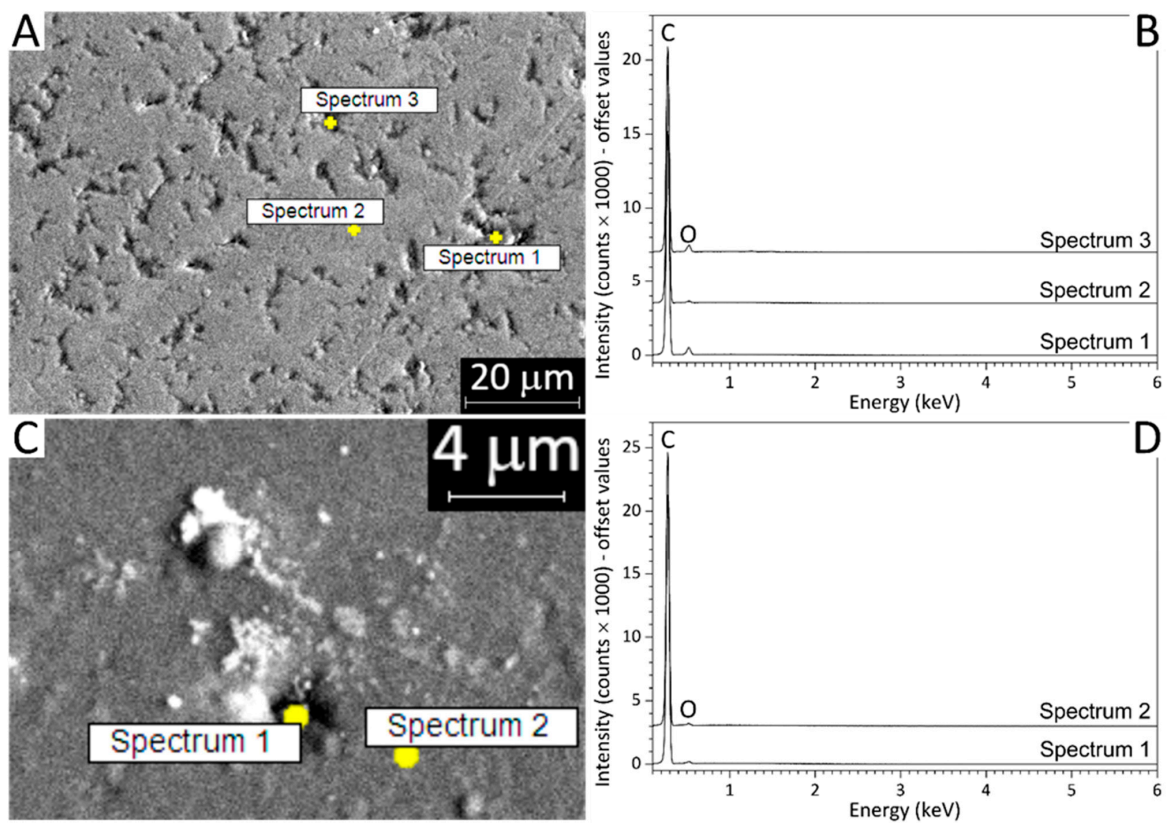


Figure 20. SEM micrographs (A,C) and corresponding EDX spectra (B,D) acquired on the sliding traces on polished DLC (A,B) and as-deposited DLC, (C,D)—10 N load, 54 cm/s speed.

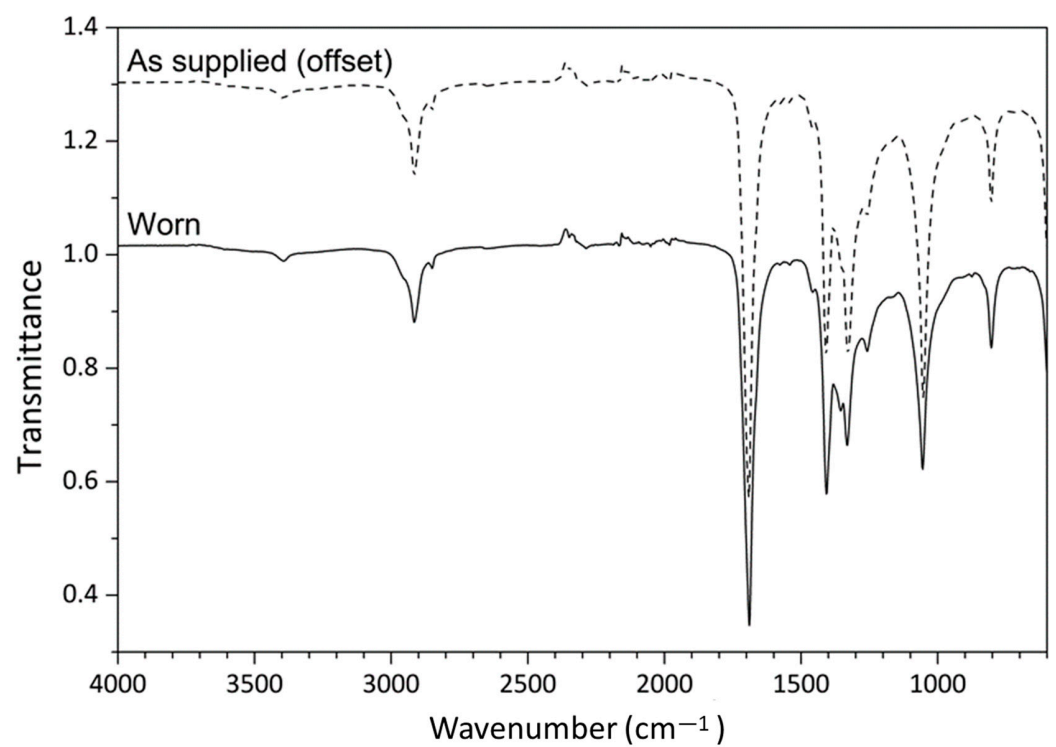


Figure 21. FTIR spectra of a polyketone pin and the worn surface of the same pin after testing against the CrN/NbN coating at 10 N load, 54 cm/s speed (spectra were offset vertically).

4. Conclusions

In this study, we compared the sliding wear behavior of a PTFE-based composite and polyketone against different counter-surfaces and under different load and speed conditions, which can be applied to rotary sealing systems for the food industry.

Through the analysis, we identified the wear mechanisms for each tribological coupling. Whether or not the polymer can transfer and maintain the tribo-layer on the antagonist is extremely important for the wear mechanism. This ability is affected by the surface texture of the counterpart. The tribo-layer can protect against wear if it is properly adhered to the countersurface. Conversely, wear increases if the tribo-layer detaches repeatedly during sliding. The effect of the tribo-layer on the coefficient of friction is more complex. With the PTFE-based composite, a stable tribo-layer was associated with lower friction, while a stable tribo-layer led to higher friction with polyketone, albeit with low wear (as previously mentioned).

Under all testing conditions, the PTFE-matrix composite produced steady-state friction coefficient values <0.2 , while values >0.5 were obtained with polyketone. However, distinct counterfaces exhibited different abilities to retain a PTFE-based tribo-layer and therefore to maintain a steady-state, low-friction regime. Polished Cr_2O_3 , which had very few protruding asperities (low S_p value) but many large valleys, due to its open porosity (a high S_v value and $S_{sk} < 0$), retained the tribo-layer throughout the test. A stable friction coefficient of between 0.15 and 0.2 was therefore retained until the end of the test, and very low specific wear rates of $1\text{--}2 \times 10^{-7} \text{ mm}^3/(\text{N}\cdot\text{m})$ were observed. By contrast, the transfer layer was removed from the surfaces with CrN/NbN or DLC-based coatings after a particular sliding distance. This triggered a transition to a higher friction ($\mu > 0.2$) regime and was associated with higher wear of the polymer composite, of between 1×10^{-6} and $5 \times 10^{-6} \text{ mm}^3/(\text{N}\cdot\text{m})$, which was mainly due to the adhesive wear of the PTFE-based matrix.

Polyketone also exhibited some adhesive wear, but ductile abrasive grooving (micro-cutting and micro-plowing) was the most damaging wear mechanism. Thus, more wear was found for polyketone when combined with a counterface that had protruding asperities (high S_p value), with wear rates $>10^{-5} \text{ mm}^3/(\text{N}\cdot\text{m})$ compared to as-deposited DLC. Polyketone also tended to form transfer layers on the counterfaces, particularly if they contained numerous valleys with a negatively skewed height distribution, as was the case for polished CrN/NbN and Cr_2O_3 . Here, the formation of a transfer layer was associated with lower wear of roughly $2\text{--}4 \times 10^{-7} \text{ mm}^3/(\text{N}\cdot\text{m})$, but with higher friction coefficients (>0.6 and sometimes approaching 1).

Author Contributions: Conceptualization: F.A., G.B., A.B., L.L.; Methodology: F.A., G.B., A.B., L.L.; Investigation: F.A., G.B., S.D.L.; Supervision: F.A., G.B., A.B., L.L.; Data curation: F.A., G.B., S.D.L.; Formal analysis: F.A., G.B., S.D.L.; Visualization: F.A., G.B.; Writing—Original draft: F.A.; Writing—Review & editing: F.A., G.B., L.L.; Project administration: A.B. and L.L.; Resources: A.B. and L.L. All authors have read and agreed to the published version of the manuscript.

Funding: This research received no external funding.

Institutional Review Board Statement: Not applicable.

Informed Consent Statement: Not applicable.

Data Availability Statement: Data are available from the authors upon request.

Conflicts of Interest: The authors declare no conflict of interest.

References

1. Ashby, M. *The CES EduPack Resource Booklet 2—Material and Process Charts*; Cambridge University: Cambridge, UK, 2009.
2. Fox, M. Polymer Tribology. *Lube Mag.* **2016**, *135*, 32–37.
3. Bhushan, B. *Principles and Applications of Tribology*, 2nd ed.; John Wiley & Sons Ltd.: Chichester, UK, 2013; ISBN 978-1-119-94454-6.
4. Straffelini, G. Materials for Tribology. In *Friction and Wear-Methodologies for Design and Control*; Springer International Publishing: Cham, Switzerland, 2015; pp. 159–199.

5. Straffelini, G. Surfaces in Contact. In *Friction and Wear-Methodologies for Design and Control*; Springer Tracts in Mechanical Engineering; Springer International Publishing: Cham, Switzerland, 2015; pp. 1–20.
6. Stachowiak, G.W.; Batchelor, A.W. Wear of Non-Metallic Materials. In *Engineering Tribology*; Elsevier: Burlington, MA, USA, 2014; pp. 679–734. ISBN 978-0-12-397047-3.
7. Biswas, S.K.; Vijayan, K. Friction and wear of PTFE—A review. *Wear* **1992**, *158*, 193–211. [[CrossRef](#)]
8. Blanchet, T.A. Wear of Polytetrafluoroethylene and PTFE composites. In *Polymer Tribology*; Sinha, S.K., Briscoe, B.J., Eds.; Imperial College Press: London, UK, 2009; pp. 347–374. ISBN 978-1-84816-202-0.
9. Friedrich, K. Polymer composites for tribological applications. *Adv. Ind. Eng. Polym. Res.* **2018**, *1*, 3–39. [[CrossRef](#)]
10. Song, F.; Wang, Q.; Wang, T. Effects of glass fiber and molybdenum disulfide on tribological behaviors and PV limit of chopped carbon fiber reinforced Polytetrafluoroethylene composites. *Tribol. Int.* **2016**, *104*, 392–401. [[CrossRef](#)]
11. Vasilev, A.P.; Okhlopkova, A.A.; Struchkova, T.S.; Grakovich, P.N.; Bashlakova, A.L. Investigation of the Influence of Complex Fillers on the Properties and Structure of Polytetrafluoroethylene. *J. Frict. Wear* **2018**, *39*, 427–432. [[CrossRef](#)]
12. Zhang, F.; Zhang, J.; Zhu, Y.; Wang, X.; Jin, Y. Microstructure and Properties of Polytetrafluoroethylene Composites Modified by Carbon Materials and Aramid Fibers. *Coatings* **2020**, *10*, 1103. [[CrossRef](#)]
13. Fan, X.; Li, G.; Guo, Y.; Zhang, L.; Xu, Y.; Zhao, F.; Zhang, G. Role of reinforcement types and silica nanoparticles on tribofilm growth at PTFE-Steel interface. *Tribol. Int.* **2020**, *143*, 106035. [[CrossRef](#)]
14. Conte, M.; Igartua, A. Study of PTFE composites tribological behavior. *Wear* **2012**, *296*, 568–574. [[CrossRef](#)]
15. Khedkar, J.; Negulescu, I.; Meletis, E.I. Sliding wear behavior of PTFE composites. *Wear* **2002**, *252*, 361–369. [[CrossRef](#)]
16. Ye, P.; Wu, J.; Mu, L.; He, D.; Feng, X.; Lu, X. Tribological behaviors of carbon series additions reinforced CF/PTFE composites at high speed. *J. Appl. Polym. Sci.* **2016**, *133*, 43236. [[CrossRef](#)]
17. Drent, E.; Mul, W.P.; Smaardijk, A.A. Polyketones. In *Encyclopedia of Polymer Science and Technology*; Wiley: Chichester, UK, 2003.
18. Unal, H.; Sen, U.; Mimaroglu, A. Dry sliding wear characteristics of some industrial polymers against steel counterface. *Tribol. Int.* **2004**, *37*, 727–732. [[CrossRef](#)]
19. Zhang, G.; Wetzel, B.; Jim, B.; Oesterle, W. Impact of counterface topography on the formation mechanisms of nanostructured tribofilm of PEEK hybrid nanocomposites. *Tribol. Int.* **2015**, *83*, 156–165. [[CrossRef](#)]
20. Bahadur, S.; Schwartz, C. Mechanical and Tribological Behavior of Polymers Filled with Particulate Fillers. In *Polymer Tribology*; Sinha, S.K., Briscoe, B.J., Eds.; Imperial College Press: London, UK, 2009; pp. 416–448.
21. Ye, J.; Tao, B.; Sun, W.; Haidar, D.R.; Alam, K.I.; Liu, K.; Burris, D.L. The Competing Effects of Counterface Peaks and Valleys on the Wear and Transfer of Ultra-Low Wear Alumina–PTFE. *Tribol. Lett.* **2018**, *66*, 12. [[CrossRef](#)]
22. Friedrich, K.; Karger-Kocsis, J.; Lu, Z. Effects of steel counterface roughness and temperature on the friction and wear of PE(E)K composites under dry sliding conditions. *Wear* **1991**, *148*, 235–247. [[CrossRef](#)]
23. Akagaki, T.; Kawabata, M. Effects of Counterface Surface Roughness on Friction and Wear of PEEK Materials under Oil-Lubricated Conditions. *Tribol. Online* **2016**, *11*, 494–502. [[CrossRef](#)]
24. Nunez, E.E.; Polycarpou, A.A. The effect of surface roughness on the transfer of polymer films under unlubricated testing conditions. *Wear* **2015**, *326–327*, 74–83. [[CrossRef](#)]
25. Suhrberg, C.H.; Pauschitz, A.; Badisch, E. Einfluss der Kontaktfläche auf den PTFE-Transfer glasfaserver stärkter PTFE-Verbundwerkstoffe. *Tribol. Schmierungstechnik* **2007**, *54*, 18–23.
26. Fontaine, J.; Donnet, C.; Erdemir, A. Fundamentals of the Tribology of DLC Coatings. In *Tribology of Diamond-Like Carbon Films*; Donnet, C., Erdemir, A., Eds.; Springer US: Boston, MA, USA, 2008; pp. 139–154.
27. Amenta, F.; Bolelli, G.; Pedrazzi, S.; Allesina, G.; Santeramo, F.; Bertarini, A.; Sassatelli, P.; Lusvardi, L. Sliding wear behaviour of fibre-reinforced PTFE composites against coated and uncoated steel. *Wear* **2021**, *486–487*, 204097. [[CrossRef](#)]
28. Bolelli, G.; Cannillo, V.; Lusvardi, L.; Manfredini, T. Wear behaviour of thermally sprayed ceramic oxide coatings. *Wear* **2006**, *261*, 1298–1315. [[CrossRef](#)]
29. Lee, D. Wear-Resistant Coatings. In *ASM Handbook-Volume 5A: Thermal Spray Technology*; Tucker, R.C., Jr., Ed.; ASM International: Materials Park, OH, USA, 2013; pp. 253–256. ISBN 978-1-61503-996-8.
30. Robertson, J. Diamond-Like Carbon Films, Properties and Applications. In *Comprehensive Hard Materials*; Sarin, V.K., Mari, D., Llanes, L., Eds.; Elsevier: Amsterdam, The Netherlands, 2014; pp. 101–139.
31. van der Kolk, G.J. Wear Resistance of Amorphous DLC and Metal Containing DLC in Industrial Applications. In *Tribology of Diamond-Like Carbon Films*; Erdemir, A., Donnet, C., Eds.; Springer: Boston, MA, USA, 2008; pp. 484–493.
32. Héau, C. DLC Films in Mechanical and Manufacturing Industry. In *Tribology of Diamond-Like Carbon Films*; Ali, E., Donnet, C., Eds.; Springer: Boston, MA, USA, 2008; pp. 469–483.
33. Hovsepian, P.E.; Lewis, D.B.; Müünz, W.-D.; Rouzaud, A.; Juliet, P. Chromium nitride/niobium nitride superlattice coatings deposited by combined cathodic-arc/unbalanced magnetron technique. *Surf. Coat. Technol.* **1999**, *116–119*, 727–734. [[CrossRef](#)]
34. Ceramic Seal Surface Rebuild and Protection. Available online: <https://www.asbindustries.com/news/127/65/Ceramic-Seal-Surface-Rebuild-and-Protection/d.FeaturedApplication> (accessed on 29 March 2021).
35. Aguiar, P.H.L.; Vidotti, S.E.; Cruz, S.A. The Effects of Accelerated Aging and Contact with Food Simulants on the Adhesion of Amorphous Hydrogenated Carbon Films Deposited on Clarified Polypropylene. *J. Adhes.* **2013**, *89*, 611–628. [[CrossRef](#)]
36. Superlattice. Available online: <https://www.lafer.eu/en/superlattice/> (accessed on 18 August 2021).

37. Kimura, Y.; Wakabayashi, T.; Okada, K.; Wada, T.; Nishikawa, H. Boron nitride as a lubricant additive. *Wear* **1999**, *232*, 199–206. [[CrossRef](#)]
38. Erdemir, A. Solid Lubricants and Self-Lubricating Films. In *Modern Tribology Handbook, Two Volume Set*; Bhushan, B., Ed.; Mechanics and Materials Science Series; CRC Press: Boca Raton, FL, USA, 2001; pp. 787–825. ISBN 9780849384035.
39. Münz, W.-D.; Lewis, D.; Creasey, S.; Hurkmans, T.; Trinh, T.; Ijzendor, W. Defects in TiN and TiAlN coatings grown by combined cathodic arc/unbalanced magnetron technology. *Vacuum* **1995**, *46*, 323–330. [[CrossRef](#)]
40. Anders, A. Approaches to rid cathodic arc plasmas of macro- and nanoparticles: A review. *Surf. Coat. Technol.* **1999**, *120–121*, 319–330. [[CrossRef](#)]
41. Chai, H.; Lawn, B.R. Fracture mode transitions in brittle coatings on compliant substrates as a function of thickness. *J. Mater. Res.* **2004**, *19*, 1752–1761. [[CrossRef](#)]
42. Lau, K.H.; Li, K.Y.; Mai, Y.W. Influence of hardness ratio on scratch failure of coatings. *Int. J. Surf. Sci. Eng.* **2007**, *1*, 3. [[CrossRef](#)]
43. Rodrigo, A.; Perillo, P.; Ichimura, H. On the correlation of substrate microhardness with the critical load of scratch adherence for hard coatings. *Surf. Coat. Technol.* **2000**, *124*, 87–92. [[CrossRef](#)]
44. Lewis, D.B.; Hovsepian, P.E.; Schönjahn, C.; Ehasarian, A.; Smith, I.J. Industrial scale manufactured superlattice hard PVD coatings. *Surf. Eng.* **2001**, *17*, 15–27.
45. Purandare, Y.; Stack, M.M.; Hovsepian, P. A study of the erosion–corrosion of PVD CrN/NbN superlattice coatings in aqueous slurries. *Wear* **2005**, *259*, 256–262. [[CrossRef](#)]
46. Hovsepian, P.E.; Lewis, D.; Münz, W.; Lyon, S.; Tomlinson, M. Combined cathodic arc/unbalanced magnetron grown CrN/NbN superlattice coatings for corrosion resistant applications. *Surf. Coat. Technol.* **1999**, *120–121*, 535–541. [[CrossRef](#)]
47. Hovsepian, P.E.; Münz, W.-D.; Medlock, A.; Gregory, G. Combined cathodic arc/unbalanced magnetron grown CrN/NbN superlattice coatings for applications in the cutlery industry. *Surf. Coat. Technol.* **2000**, *133–134*, 508–516. [[CrossRef](#)]
48. Henda, R.; Wilson, G.; Gray-Munro, J.; Alshekhi, O.; McDonald, A.M. Preparation of polytetrafluoroethylene by pulsed electron ablation: Deposition and wettability aspects. *Thin Solid Films* **2012**, *520*, 1885–1889. [[CrossRef](#)]
49. Wang, M.; Cheng, J.; Li, M.; He, F. Structure and properties of soda lime silicate glass doped with rare earth. *Phys. B Condens. Matter* **2011**, *406*, 187–191. [[CrossRef](#)]
50. Abdelghany, A.M.; ElBatal, F.H.; ElBatal, H.A.; EzzElDin, F.M. Optical and FTIR structural studies of CoO-doped sodium borate, sodium silicate and sodium phosphate glasses and effects of gamma irradiation—a comparative study. *J. Mol. Struct.* **2014**, *1074*, 503–510. [[CrossRef](#)]
51. Taylor, W.R. Application of infrared spectroscopy to studies of silicate glass structure: Examples from the melilite glasses and the systems Na₂O–SiO₂ and Na₂O–Al₂O₃–SiO₂. *J. Earth Syst. Sci.* **1990**, *99*, 99–117. [[CrossRef](#)]
52. Rodiouchkina, M.; Lind, J.; Pelcastre, L.; Berglund, K.; Rudolphi, Å.K.; Hardell, J.; Kassman, Å.; Hardell, J.; Rudolphi, Å.K.; Hardell, J. Tribological behaviour and transfer layer development of self-lubricating polymer composite bearing materials under long duration dry sliding against stainless steel. *Wear* **2021**, *484–485*, 204027. [[CrossRef](#)]
53. Zuo, Z.; Yang, Y.; Qi, X.; Su, W.; Yang, X. Analysis of the chemical composition of the PTFE transfer film produced by sliding against Q235 carbon steel. *Wear* **2014**, *320*, 87–93. [[CrossRef](#)]
54. Onodera, T.; Kawasaki, K.; Nakakawaji, T.; Higuchi, Y.; Ozawa, N.; Kurihara, K.; Kubo, M. Effect of Tribochemical Reaction on Transfer-Film Formation by Poly(tetrafluoroethylene). *J. Phys. Chem. C* **2014**, *118*, 11820–11826. [[CrossRef](#)]
55. Klaas, N.V.; Marcus, K.; Kellock, C. The tribological behaviour of glass filled polytetrafluoroethylene. *Tribol. Int.* **2005**, *38*, 824–833. [[CrossRef](#)]
56. Shkrabo, D.M.; Zhizhin, G.N.; Kuzik, L.A.; Garbuzova, I.A. The ethylene–carbon monoxide copolymer (‘Carilon’) vibrational spectra and study of nanometer films on gold covered substrate. *Vib. Spectrosc.* **1998**, *17*, 155–162. [[CrossRef](#)]